Quantum Error Modelling and Correction in Long Distance Teleportation using Singlet States

by

Joe Aung

Submitted to the Department of Electrical Engineering and Computer Science
in partial fulfillment of the requirements for the degree of

Master of Science in Electrical Engineering and Computer Science

at the

MASSACHUSETTS INSTITUTE OF TECHNOLOGY

May 2002
[June 2002]

Author .....
Department of Electrical Engineering and Computer Science
May 21, 2002

Certified by .....
Jeffrey H. Shapiro
Julius A. Stratton Professor of Electrical Engineering
Director, Research Laboratory for Electronics
Thesis Supervisor

Accepted by .....
Arthur C. Smith
Chairman, Department Committee on Graduate Students

Quantum Error Modelling and Correction in Long Distance Teleportation using Singlet States

by

Joe Aung

Submitted to the Department of Electrical Engineering and Computer Science
on May 21, 2002, in partial fulfillment of the
requirements for the degree of
Master of Science in Electrical Engineering and Computer Science

Abstract

Under a multidisciplinary university research initiative (MURI) program, researchers at the Massachusetts Institute of Technology (MIT) and Northwestern University (NU) are developing a long-distance, high-fidelity quantum teleportation system. This system uses a novel ultrabright source of entangled photon pairs and trapped-atom quantum memories. This thesis will investigate the potential teleportation errors involved in the MIT/NU system. A single-photon, Bell-diagonal error model is developed that allows us to restrict possible errors to just four distinct events. The effects of these errors on teleportation, as well as their probabilities of occurrence, are determined. Techniques drawn from quantum error correcting codes and entanglement purification protocols are investigated as means for reducing teleportation errors in the MIT/NU architecture. Finally we apply existing bounds on the achievable rate of reliable quantum communication to the MIT/NU system.

Thesis Supervisor: Jeffrey H. Shapiro
Title: Julius A. Stratton Professor of Electrical Engineering
Director, Research Laboratory for Electronics

Acknowledgments

First, I must thank my research advisor Professor Jeffrey H. Shapiro. He gave me the opportunity to work in the quantum MURI group and throughout my time in graduate school he has continually provided direction as well as invaluable advice and instruction.

My parents and brother have always been there when I've need them. I am grateful to them for their encouragement and also for helping me keep things in perspective. I thank Brent Yen for numerous interesting and helpful discussions while I was writing my thesis. Finally, I thank Anne for all the great times we've shared over the last two years. She has made the graduate school workload much easier to bear.

This work was supported by the DoD Multidisciplinary University Research Initiative (MURI) program administered by the Army Research Office under Grant DAAD19-00-1-0177.

Contents

Chapter 1

Introduction

In 1993, Bennett et al [1] described a method for using a pair of particles entangled in a singlet state to transmit an unknown quantum state from a sender to a receiver. This unknown state is destroyed at the sender and recreated at the receiver. The procedure was dubbed "quantum teleportation". In 1997, a team led by Dr. Anton Zeilinger at the University of Innsbruck achieved the first experimental success in teleportation using a polarized single photon for the arbitrary quantum state. The Innsbruck experiment only teleported states over short distances and was unable to store them as it lacked a quantum memory element.

A team of researchers from the Massachusetts Institute of Technology (MIT) and Northwestern University (NU), led by Prof. Jeffrey Shapiro, is now developing a quantum communication system capable of long-distance, high-fidelity teleportation. This system, whose architecture is described in [2], uses a novel ultrabright source of polarization-entangled photon pairs [3] and trapped-atom quantum memories [4]. Preliminary analysis, limited only by loss, suggests it may be capable of throughputs as high as 500 pairs/sec over 50 km end-to-end paths at 95% fidelity. Even without generalizing this analysis to include a variety of phase-error mechanisms, there are significant performance issues to be addressed. Addressing such issues will be the focus of the proposed thesis.

The success of the Bennett et al. teleportation scheme requires that the transmitter and receiver share a singlet state. In the MIT/NU architecture, however, the transmitter and receiver are in a mixed state [2]. Thus, although this mixed state contains a strong singlet component, there is a finite probability that an error will occur when teleporting a photon

state using this system. The objective of the proposed thesis is to develop a quantum channel model for the noisy teleportation process and to seek methods for reducing the occurrence and/or correcting the effects of the resulting teleportation errors. In particular, we present and compare two methods of reducing teleportation errors: 1. Quantum Error Correcting Codes (QECC) [5], [6], 2. Entanglement Purification Protocols (EPP) [7], [8].

The importance of QECC and EPP techniques for mitigating quantum errors extends to the wider context of quantum computing. Attempts to realize quantum computers have run up against fundamental problems in maintaining the coherence of quantum systems. Whereas classical systems are stable due to the large relative size of the system as compared to environmental perturbations, quantum systems that use single atoms, photons, or electrons are much more sensitive to fluctuations in the physical environment. Indeed, practical implementations of quantum gates have not achieved accuracies greater than 90% [9], whereas quantum factoring of numbers large enough to be difficult for classical computers requires accuracies of one part in a billion [9]. Quantum error correcting codes and entanglement purification protocols may be ways of getting closer to the required limits.

Successful removal of quantum errors would lead the way to some remarkable applications of quantum computers and information systems such as:

Searching: Algorithmic searching. Grover's quantum search algorithm allows us to find an item in an unstructured search space of size N in $\sqrt{N}$ operations [10] (Classical algorithms require N operations).

Factoring: Prime factorization of large numbers in polynomial time. Shor's algorithm allows large numbers to be factored efficiently on a quantum computer [11] (Classical algorithms have an exponential growth rate for such factoring problems).

Simulation: Simulating quantum systems efficiently. In analogy to Turing's suggestion that any algorithmic process can be simulated efficiently using a classical computer, perhaps quantum computers can naturally simulate quantum systems efficiently [11].

Interest in these applications has inspired considerable work on quantum error correcting codes and entanglement purification protocols. The proposed thesis will apply these efforts in the specific context of the MIT/NU teleportation architecture.

We will begin in Chapter 2 by reviewing the basic concepts in quantum information theory required to read this thesis. This includes quantum states and transformations,

entanglement, teleportation and mixed states. In Chapter 3, we will describe the MIT/NU teleportation architecture. In Chapter 4, we will develop an error model for our system. We show that the removal of multiphoton errors allow us to model the teleportation of a qubit as the transmission of a qubit through a depolarizing channel. Finally, in Chapter 5, we review existing entanglement purification protocols and error correcting codes, we analyze their application to the MIT/NU system and apply existing limits on the rate of reliable quantum communication to the depolarizing channel model for the MIT/NU system.

Chapter 2

Background Information

For analysis of the MIT/NU teleportation system and the application of error correcting techniques to it, we will require a background knowledge of quantum information theory. In this chapter we will summarize the basic concepts required to understand the remainder of this thesis.

2.1 Qubits and Quantum Transformations

Since we will be interested in quantum communication, we will first introduce the basic unit of quantum information - the qubit. The qubit is the quantum mechanical analog of the classical bit. Whereas classical bits can take on state values of either 0 or 1, a qubit can take on the states $|1\rangle$, $|0\rangle$ or a linear combination state; i.e., the general state of qubit is

$$|\psi\rangle = \alpha|0\rangle + \beta|1\rangle, \tag{2.1}$$

where α and β are complex numbers satisfying $|\alpha|^2 + |\beta|^2 = 1$. When we make a quantum measurement on the state of the qubit, we get the result 0 with probability $|\alpha|^2$ and 1 with probability $|\beta|^2$.

Geometrically, a qubit can be represented as a unit vector in a two-dimensional complex vector space in the following manner:

$$|\psi\rangle = \begin{bmatrix} \alpha \\ \beta \end{bmatrix}, \tag{2.2}$$

with $|0\rangle$ and $|1\rangle$ as the basis states.

If we are interested in the state of multiple qubits, more basis states are needed. A system of n qubits requires 2^n basis states. For example, the state of a system of two qubits can be represented in terms of four basis states: $|00\rangle$, $|01\rangle$, $|10\rangle$, $|11\rangle$. Such a two qubit system generally exists in a superposition of these four states:

$$|\psi\rangle = \alpha_{00}|00\rangle + \alpha_{01}|01\rangle + \alpha_{10}|10\rangle + \alpha_{11}|11\rangle, \tag{2.3}$$

where $|\alpha_{00}|^2 + |\alpha_{01}|^2 + |\alpha_{10}|^2 + |\alpha_{11}|^2 = 1$. Again, the geometric picture is a unit vector, this time in four-dimensional complex vector space.

The evolution of the state vector describing an isolated quantum system occurs in a linear and inner-product conserving manner. Mathematically, it is said to undergo a unitary transformation.

Now, in analogy to classical computation, where any operation can be described by a combination of one and two-bit logic gates (NOT, AND), quantum operations can be expressed as a sequence of one and two-qubit quantum logic gates [12].

In general, a quantum logic gate $\hat{U} = \begin{bmatrix} a & b \\ c & d \end{bmatrix}$ acts on a qubit $|\psi\rangle = \alpha|0\rangle + \beta|1\rangle = \begin{bmatrix} \alpha \\ \beta \end{bmatrix}$ as follows:

$$\hat{U}|\psi\rangle = \begin{bmatrix} a & b \\ c & d \end{bmatrix} \begin{bmatrix} \alpha \\ \beta \end{bmatrix} = \begin{bmatrix} \alpha a + \beta b \\ \alpha c + \beta d \end{bmatrix}, \tag{2.4}$$

thus mapping $|0\rangle$ to $a|0\rangle + c|1\rangle$ and $|1\rangle$ to $b|0\rangle + d|1\rangle$. Here, $\hat{U}$ is a unitary matrix satisfying $\hat{U}^\dagger\hat{U} = \hat{I}$, where

$$\hat{U}^{\dagger} = \begin{bmatrix} a^* & c^* \\ b^* & d^* \end{bmatrix}, \tag{2.5}$$

$$\hat{I} = \begin{bmatrix} 1 & 0 \\ 0 & 1 \end{bmatrix}. \tag{2.6}$$

The standard one-qubit gates are represented by 2×2 unitary matrices. Three important operations are described by the Pauli matrices:

$$\hat{\sigma}_x \equiv \begin{bmatrix} 0 & 1 \\ 1 & 0 \end{bmatrix}; \hat{\sigma}_y \equiv \begin{bmatrix} 0 & -i \\ i & 0 \end{bmatrix}; \hat{\sigma}_z \equiv \begin{bmatrix} 1 & 0 \\ 0 & -1 \end{bmatrix}. \tag{2.7}$$

$\hat{\sigma}_x$ acts as a bit-flip on a qubit, $\hat{\sigma}_z$ acts as a phase-flip and $\hat{\sigma}_y$ acts by applying both a bit-flip and a phase-flip.

The standard two-qubit gate is the quantum exclusive or (XOR), otherwise known as the CNOT (controlled NOT):

$$\hat{X} \equiv \begin{bmatrix} 1 & 0 & 0 & 0 \\ 0 & 1 & 0 & 0 \\ 0 & 0 & 0 & 1 \\ 0 & 0 & 1 & 0 \end{bmatrix}. \tag{2.8}$$

Writing (2.3) in vector form

$$|\psi\rangle = \begin{bmatrix} \alpha_{00} \\ \alpha_{01} \\ \alpha_{10} \\ \alpha_{11} \end{bmatrix} \tag{2.9}$$

where the first index represents the source qubit and the second index represents the target qubit we see that $\hat{X}$ flips the target qubit if the source qubit is $|1\rangle$ and does nothing if the source qubit is $|0\rangle$.

The set of one-qubit gates and the CNOT gate form a basic set of operations from which any quantum operation can be built [12].

2.1.1 No-Cloning theorem

Now that we have introduced qubits and quantum operations, we will state an important property of quantum information that is captured in the No-Cloning theorem [13]. This theorem has an important impact on quantum communication because it implies that when the transmitter sends a qubit to the receiver, a copy of the qubit cannot be left with the sender.

The No-Cloning theorem states that *there is no quantum operation that takes a general quantum state* $|\psi\rangle$ *to* $|\psi\rangle|\psi\rangle$.

This is fact is a simple consequence of the linearity of quantum mechanics. To illustrate this, consider a quantum operation $\hat{U}$ that *copies* a source state $|s\rangle$ into a target state $|t\rangle$ as follows:

$$\hat{U}|s\rangle \otimes |t\rangle = |s\rangle \otimes |s\rangle. \tag{2.10}$$

This operation would copy two distinct states $|\psi\rangle$ and $|\phi\rangle$ as follows:

$$\hat{U}|\psi\rangle \otimes |t\rangle = |\psi\rangle \otimes |\psi\rangle, \tag{2.11}$$

$$\hat{U}|\phi\rangle \otimes |t\rangle = |\phi\rangle \otimes |\phi\rangle. \tag{2.12}$$

Taking the inner product of (2.11) and (2.12) gives

$$\langle\psi|\phi\rangle = (\langle\psi|\phi\rangle)^2. \tag{2.13}$$

This equation only has two solutions. Either $|\psi\rangle = |\phi\rangle$ or the two states are orthogonal. This shows that there is no quantum operation that can clone a general quantum state.

2.2 Entanglement and Bell States

Entanglement is the crucial property of bipartite quantum systems that makes teleportation possible. The notion of entanglement was brought into focus in a paper by Einstein, Podolsky and Rosen [14] that described the non-local nature of quantum mechanics.

A pure state $|\psi\rangle_{AB}$ is said to be entangled if it cannot be written as a tensor product of its parts $|\psi\rangle_A \otimes |\psi\rangle_B$. The entanglement of a pure state $|\psi\rangle_{AB}$ is quantitatively

$$E(\psi) = S(\hat{\rho}_A) = S(\hat{\rho}_B), \tag{2.14}$$

where $S(\hat{\rho}) = -\mathrm{Tr}\,(\hat{\rho}\log_2\hat{\rho})$ is called the von Neumann entropy and $\hat{\rho}_A = \mathrm{Tr}_B\,(|\psi\rangle_{AB\,AB}\langle\psi|)$ is the reduced density matrix obtained by taking the partial trace of the density matrix of $|\psi\rangle_{AB}$ over B.

In many ways, entanglement can be regarded as a natural resource in the same way as energy or information. Entangled particles cannot be created out of non-entangled particles and in general, you cannot increase the entanglement of a bipartite quantum system with local operations on the subparts [7].

There are other properties of entanglement worth noting:

- The entanglement E of a two particle system ranges from zero for a product state to $E = 1$ for the singlet state. The standard unit of entanglement is the *ebit*, defined as the amount of entanglement in a singlet.

- Entanglement is additive, meaning a system of n singlets will have n ebits of entanglement.

An important class of entangled two-qubit states are the Bell states. These states can be obtained by the rotation of the computational two-qubit basis $|00\rangle$, $|01\rangle$, $|10\rangle$, $|11\rangle$. The result is another set of four orthonormal basis states, known as the Bell basis:

$$|\Psi^-\rangle = \frac{1}{\sqrt{2}}(|01\rangle - |10\rangle), \tag{2.15}$$

$$|\Psi^+\rangle = \frac{1}{\sqrt{2}}(|01\rangle + |10\rangle), \tag{2.16}$$

$$|\Phi^-\rangle = \frac{1}{\sqrt{2}}(|00\rangle - |11\rangle), \tag{2.17}$$

$$|\Phi^+\rangle = \frac{1}{\sqrt{2}}(|00\rangle + |11\rangle). \tag{2.18}$$

The first state $|\Psi^-\rangle$ is called the singlet state and the other three are known as the triplet states. These names for the states derive from the number of ways spins can couple in a two-particle quantum system.

Bell states map onto one another under 3 sets of operations defined in Tables 2.1, 2.2 and 2.3. Each of the unilateral rotations are performed by applying one of the Pauli matrices to either (but only one) half of the pair. Bilateral $\pi/2$ rotations are defined by the following matrices:

$$\hat{I} = \begin{bmatrix} 1 & 0 \\ 0 & 1 \end{bmatrix} \otimes \begin{bmatrix} 1 & 0 \\ 0 & 1 \end{bmatrix}, \tag{2.19}$$

$$\hat{B}_x = \begin{bmatrix} \frac{1}{\sqrt{2}} & \frac{i}{\sqrt{2}} \\ \frac{i}{\sqrt{2}} & \frac{1}{\sqrt{2}} \end{bmatrix} \otimes \begin{bmatrix} \frac{1}{\sqrt{2}} & \frac{i}{\sqrt{2}} \\ \frac{i}{\sqrt{2}} & \frac{1}{\sqrt{2}} \end{bmatrix}, \tag{2.20}$$

$$\hat{B}_y = \begin{bmatrix} \frac{1}{\sqrt{2}} & \frac{1}{\sqrt{2}} \\ \frac{-1}{\sqrt{2}} & \frac{1}{\sqrt{2}} \end{bmatrix} \otimes \begin{bmatrix} \frac{1}{\sqrt{2}} & \frac{1}{\sqrt{2}} \\ \frac{-1}{\sqrt{2}} & \frac{1}{\sqrt{2}} \end{bmatrix}, \tag{2.21}$$

$$\hat{B}_z = \begin{bmatrix} e^{i\pi/4} & 0 \\ 0 & e^{i\pi/4} \end{bmatrix} \otimes \begin{bmatrix} e^{i\pi/4} & 0 \\ 0 & e^{i\pi/4} \end{bmatrix}, \tag{2.22}$$

where we have explicitly written the bilateral rotations as tensor products of their actions on the separate halves of the pair. Finally, the bilateral XOR is performed by applying two instances of the unilateral XOR cf. (2.8), one on each qubit.

2.3 Singlet-Based Teleportation

Quantum teleportation uses entanglement between a *transmitter* and a *receiver* to transmit an unknown quantum state — the message, $|\psi\rangle_{\mathrm{M}}$ between the two. Assuming that the

	Source			
	Ψ^-	Φ^-	Φ^+	Ψ^+
$\hat{I}$	Ψ^-	Φ^-	Φ^+	Ψ^+
$\hat{\sigma}_x$	Φ^-	Ψ^-	Ψ^+	Φ^+
$\hat{\sigma}_y$	Φ^+	Ψ^+	Ψ^-	Φ^-
$\hat{\sigma}_z$	Ψ^+	Φ^+	Φ^-	Ψ^-

Table 2.1: Unilateral π rotations

	Source			
	Ψ^-	Φ^-	Φ^+	Ψ^+
$\hat{I}$	Ψ^-	Φ^-	Φ^+	Ψ^+
$\hat{B_x}$	Ψ^-	Φ^-	Ψ^+	Φ^+
$\hat{B_y}$	Ψ^-	Ψ^+	Φ^+	Φ^-
$\hat{B_z}$	Ψ^-	Φ^+	Φ^-	Ψ^+

Table 2.2: Bilateral $\pi/2$ rotations

	Source				
Target	Ψ^-	Φ^-	Φ^+	Ψ^+	
	Ψ^+	Φ^+	Φ^-	Ψ^-	(source)
Ψ^-	Φ^-	Ψ^-	Ψ^-	Φ^-	(target)
	Ψ^+	Φ^+	Φ^-	Ψ^-	(source)
Φ^-	Ψ^-	Φ^-	Φ^-	Ψ^-	(target)
	Ψ^-	Φ^-	Φ^+	Ψ^+	(source)
Φ^+	Ψ^+	Φ^+	Φ^+	Ψ^+	(target)
	Ψ^-	Φ^-	Φ^+	Ψ^+	(source)
Ψ^+	Φ^+	Ψ^+	Ψ^+	Φ^+	(target)

Table 2.3: Bilateral XOR

transmitter and the receiver share an entangled state $|\mathrm{TR}\rangle$, teleportation proceeds as follows:

1. The transmitter makes a joint measurement on the transmitter and $|\psi\rangle_{\mathrm{M}}$, collapsing the joint state of the entire transmitter, receiver and message system.

2. The transmitter sends a classical message to the receiver relaying the result of this measurement.

3. The receiver makes a transformation on the receiver to regenerate $|\psi\rangle$.

There are several points to take note of here:

- Step 2 of the process ensures that the procedure cannot be used to transmit information faster than the speed of light.

- No quantum information is cloned, as the state on the transmitter's side is destroyed in the measurement process.

- Neither the transmitter, nor the receiver ever finds out the state $|\psi\rangle_{\mathrm{M}}$.

To make the above procedure more explicit, consider the Bennett protocol, in which the transmitter and the receiver share a singlet state $|\Psi^-\rangle = \frac{1}{\sqrt{2}}(|01\rangle_{\mathrm{TR}} - |10\rangle_{\mathrm{TR}})$. Suppose the transmitter wants to teleport the quantum message $|\psi\rangle_{\mathrm{M}} = a|0\rangle_{\mathrm{M}} + b|1\rangle_{\mathrm{M}}$. The joint state of the entire system is:

$$
\begin{aligned}
|\psi\rangle_{\mathrm{TR}}|\psi\rangle_{\mathrm{M}} &= \frac{1}{\sqrt{2}}(|01\rangle_{\mathrm{TR}} - |10\rangle_{\mathrm{TR}})(a|0\rangle_{\mathrm{M}} + b|1\rangle_{\mathrm{M}}) \\
&= \frac{a}{\sqrt{2}}(|0\rangle_{\mathrm{T}}|1\rangle_{\mathrm{R}}|0\rangle_{\mathrm{M}} - |1\rangle_{\mathrm{T}}|0\rangle_{\mathrm{R}}|0\rangle_{\mathrm{M}}) \\
&\quad + \frac{b}{\sqrt{2}}(|0\rangle_{\mathrm{T}}|1\rangle_{\mathrm{R}}|1\rangle_{\mathrm{M}} - |1\rangle_{\mathrm{T}}|0\rangle_{\mathrm{R}}|1\rangle_{\mathrm{M}}) \qquad (2.23) \\
&= \frac{1}{\sqrt{8}}(-|1\rangle_{\mathrm{T}}|0\rangle_{\mathrm{M}} + |0\rangle_{\mathrm{T}}|1\rangle_{\mathrm{M}})(a|0\rangle_{\mathrm{R}} + b|1\rangle_{\mathrm{R}}) \\
&\quad + \frac{1}{\sqrt{8}}(|1\rangle_{\mathrm{T}}|0\rangle_{\mathrm{M}} + |0\rangle_{\mathrm{T}}|1\rangle_{\mathrm{M}})(-a|0\rangle_{\mathrm{R}} + b|1\rangle_{\mathrm{R}}) \\
&\quad + \frac{1}{\sqrt{8}}(|1\rangle_{\mathrm{T}}|1\rangle_{\mathrm{M}} - |0\rangle_{\mathrm{T}}|0\rangle_{\mathrm{M}})(-a|1\rangle_{\mathrm{R}} - b|0\rangle_{\mathrm{R}}) \\
&\quad + \frac{1}{\sqrt{8}}(|1\rangle_{\mathrm{T}}|1\rangle_{\mathrm{M}} + |0\rangle_{\mathrm{T}}|0\rangle_{\mathrm{M}})(a|1\rangle_{\mathrm{R}} - b|0\rangle_{\mathrm{R}}), \qquad (2.24)
\end{aligned}
$$

where in the last step we have factored out the Bell-states between the transmitter and the state to be teleported. Thus we can write:

$$\begin{aligned}|\psi\rangle_{\mathrm{TRM}} &= \frac{1}{2}|\Psi^-\rangle_{\mathrm{TM}}(a|0\rangle_{\mathrm{R}} + b|1\rangle_{\mathrm{R}}) \\ &+\frac{1}{2}|\Psi^+\rangle_{\mathrm{TM}}(-a|0\rangle_{\mathrm{R}} + b|1\rangle_{\mathrm{R}}) \\ &+\frac{1}{2}|\Phi^-\rangle_{\mathrm{TM}}(+a|1\rangle_{\mathrm{R}} + b|0\rangle_{\mathrm{R}}) \\ &+\frac{1}{2}|\Phi^+\rangle_{\mathrm{TM}}(a|1\rangle_{\mathrm{R}} - b|0\rangle_{\mathrm{R}}). \end{aligned} \tag{2.25}$$

The transmitter now makes a measurement on $|\psi\rangle_{\mathrm{TM}}$, the joint state of the transmitter and the message, using the Bell state basis. The result of this measurement is one of the Bell states, collapsing the joint state of the entire system into one of the terms in (2.25). The transmitter then relays this result to the receiver via a two-bit classical message: $|\Psi^-\rangle_{\mathrm{TM}} = 00$, $|\Psi^+\rangle_{\mathrm{TM}} = 01$, $|\Phi^-\rangle_{\mathrm{TM}} = 10$, $|\Phi^+\rangle_{\mathrm{TM}} = 11$. Upon receipt of the transmitter's message, the receiver knows what transformation must be done to its half of the original singlet in order to regenerate the quantum message. The four transformations can be achieved using the Pauli matrices (2.7), $\hat{I}$, $\hat{\sigma}_x$, $\hat{\sigma}_y$ and $\hat{\sigma}_z$:

$$00 \rightarrow \hat{I}|\psi\rangle_{\mathrm{R}} = a|0\rangle_{\mathrm{R}} + b|1\rangle_{\mathrm{R}}, \tag{2.26}$$

$$01 \rightarrow -\hat{\sigma}_z|\psi\rangle_{\mathrm{R}} = a|0\rangle_{\mathrm{R}} + b|1\rangle_{\mathrm{R}}, \tag{2.27}$$

$$10 \rightarrow \hat{\sigma}_x|\psi\rangle_{\mathrm{R}} = a|0\rangle_{\mathrm{R}} + b|1\rangle_{\mathrm{R}}, \tag{2.28}$$

$$11 \rightarrow \hat{\sigma}_x\hat{\sigma}_z|\psi\rangle_{\mathrm{R}} = a|0\rangle_{\mathrm{R}} + b|1\rangle_{\mathrm{R}}. \tag{2.29}$$

After performing the appropriate operation, the receiver is left with a replica of the message in the receiver, $|\psi\rangle_{\mathrm{R}} = a|0\rangle_{\mathrm{R}} + b|1\rangle_{\mathrm{R}}$, whereas the transmitter is left with the two other particles in one of the states $|\Psi^{\mp}\rangle_{\mathrm{TM}}$ or $|\Phi^{\mp}\rangle_{\mathrm{TM}}$. Note that neither the transmitter, nor the receiver have learned anything about the message state $|\psi\rangle_{\mathrm{M}}$ in accordance with the no-cloning theorem of quantum mechanics [13].

2.4 Mixed States and Werner States

A mixed state is defined by its density operator

$$\hat{\rho} = \sum_i p_i |\psi_i\rangle\langle\psi_i| \tag{2.30}$$

where $\sum_i p_i = 1$ and p_i is the classical probability that the state is $|\psi_i\rangle$.

For a two-qubit system, the density operator for one of its sub-parts can be obtained by evaluating a partial trace over the other component. The partial trace of $\hat{\rho}_{AB} = |a_1 b_1\rangle\langle a_1 b_1|$ over B is defined as

$$\mathrm{tr}_B(|a_1 b_1\rangle\langle a_1 b_1|) = |a_1\rangle\langle a_2|(\langle b_1|b_2\rangle). \tag{2.31}$$

Werner states are a class of mixed states that we will encounter in the analysis of our teleportation system and in the analysis of error correcting techniques. These are classical mixtures of the four Bell states that have the following density operator

$$\hat{\rho}_{W_F} = F|\Psi^-\rangle\langle\Psi^-| + \frac{1-F}{3}\left(|\Psi^+\rangle\langle\Psi^+| + |\Phi^-\rangle\langle\Phi^-| + |\Phi^+\rangle\langle\Phi^+|\right). \tag{2.32}$$

This state is a Ψ^- Werner state. It can be prepared by drawing from a collection of states that is $x = (4F-1)/3$ parts pure singlet and $1-x$ completely mixed, for $\frac{1}{4} \leq F \leq 1$. It is also possible to swap the Ψ^- component with any of the three triplets to give us Ψ^+, Φ^- or Φ^+ Werner states.

Chapter 3

A Long-Distance, High-Fidelity Teleportation System Architecture

The MIT/NU architecture for long-distance, high-fidelity teleportation uses polarization entangled photons and long-duration quantum storage in trapped-atom quantum memories [2], as sketched in Figure 3-1.

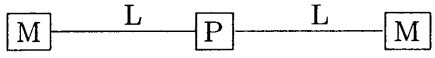

Figure 3-1: Schematic of long-distance quantum communication system: P=ultrabright narrowband source of polarization-entangled photon pairs; $L = L$ km of standard telecommunication fiber; M=trapped-atom quantum memory.

The two memories, M at either end in Figure 3-1, act as the transmitter and receiver end points for teleportation.

The ultrabright source [3], P, consists of two coherently pumped optical parametric amplifiers (OPAs). It produces pairs of polarization entangled photons — single pairs are produced in singlet states. The individual members of a pair are sent down optical fiber[1] towards the memories.

The quantum state of the pair is transferred to atomic level coherence in trapped ^{87}Rb atom quantum memory [4]. Schematics of the source and memory are shown in Figure

[1]Using quantum frequency conversion and time-division multiplexing polarization restoration permits the use of standard telecommunication fiber in this architecture.

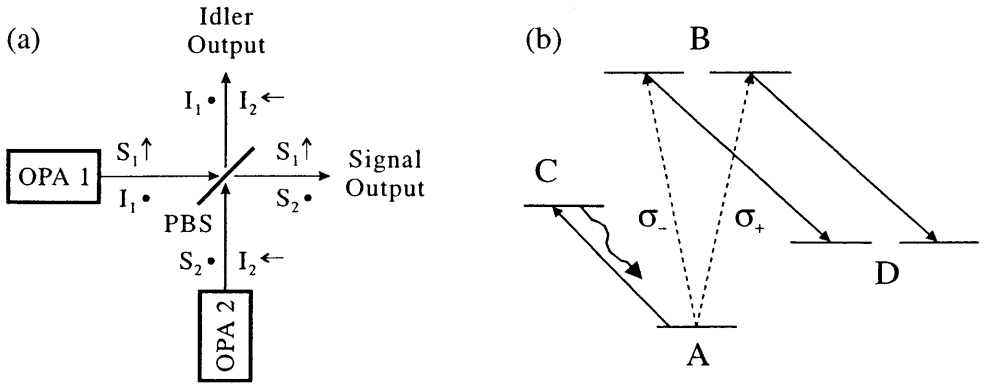

Figure 3-2: The source and memory for the quantum communication system. The source consists of two type-II phase matched optical parametric amplifiers. The polarizations of the beams in $\hat{x}$ and $\hat{y}$ directions are indicated by arrows and bullets. The trapped rubidium atom quantum memory has the energy levels shown. A-to-B transitions occurs when a photon is absorbed. B-to-D transitions are coherently driven to enable storage in the long lived D levels. The A-to-C cycling transition is used for non-destructive verification of a loading event.

3-2. The loading of a memory can be verified non-destructively with A-to-C cycling transition depicted in Figure 3-2. Once both memories are loaded, Bell measurements and the transformations required for teleportation can be made in the memories.

3.1 Memory Loading Protocol

The memories are loaded via the following protocol. Signal and idler photons travel every 400 ns down optical fibres to the quantum memories. The atoms start optically detuned or physically displaced so that no A-to-B absorptions occur but after a loading interval of 400 ns, the atoms are tuned or moved into the absorbing positions and the B-to-D coherent pumping is initiated. After 100 ns we stop coherent pumping and repeatedly drive the A-to-C cycling transition. We monitor the memory cavities for fluorescence from this transition to determine whether or not a photon was absorbed by the cavities. If either atom failed to absorb a photon, we cycle both atoms back to their A states and start the protocol again.

This protocol has been predicted to run at rates as high as 500 kHz; i.e. we can run 500,000 independent loading attempts each second. For every attempt at loading the memories, there are three possible outcomes. If at least one of the memories fails to absorb a photon we have an erasure. If both memories absorb a photon from the same entangled pair, we have a success. If both memories absorb a photon but not from the same entangled

pair, we have an error. We will denote the probabilities of these events by $p_{erasure}$, $p_{success}$ and p_{error} with

$$p_{erasure} >> p_{success} >> p_{error}, \tag{3.1}$$

under typical operating conditions.

3.2 Lossless Operation

Successful teleportation of a qubit requires that the transmitter and receiver are entangled in the singlet state. Shapiro [2] has shown that, under ideal lossless conditions, the signal photon field at frequency $\omega_S + \Delta\omega$ and the idler photon field at frequency $\omega_I - \Delta\omega$ that are produced by the dual OPA source are in the entangled Bose-Einstein state[2]:

$$|\psi\rangle_{SI} = \sum_{n=0}^{\infty} \sqrt{\frac{\overline{N}^n}{(\overline{N}+1)^{n+1}}} |n\rangle_{S_x} |n\rangle_{I_y} \sum_{n=0}^{\infty} (-1)^n \sqrt{\frac{\overline{N}^n}{(\overline{N}+1)^{n+1}}} |n\rangle_{S_y} |n\rangle_{I_x} \tag{3.2}$$

where $\overline{N} = 4G^2/[(1-G^2-\Delta\omega^2/\Gamma^2)^2 + 4\Delta\omega^2/\Gamma^2]$ is the average photon number per mode at detuning $\Delta\omega$, G is the normalized OPA gain ($G^2 = 1$ at oscillation threshold), and Γ is the OPA cavity linewidth.

For the teleportation system shown in Figure 3-1, we assume degenerate OPA operation with $\omega_S = \omega_I$ matching the 795nm line of the trapped-Rb quantum memory. Also, the OPAs are run at low gain, for which $\overline{N} << 1$ implies that,

$$\begin{aligned} |\psi\rangle_{SI} &= \frac{1}{\overline{N}+1} |0\rangle_{S_x} |0\rangle_{I_y} |0\rangle_{S_y} |0\rangle_{I_x} \\ &\quad + \sqrt{\frac{\overline{N}}{(\overline{N}+1)^3}} (|1\rangle_{S_x} |1\rangle_{I_y} |0\rangle_{S_y} |0\rangle_{I_x} - |0\rangle_{S_x} |0\rangle_{I_y} |1\rangle_{S_y} |1\rangle_{I_x}), \end{aligned} \tag{3.3}$$

to lowest non-vacuum order. Equation (3.3) shows that $|\psi\rangle_{SI}$ is mostly vacuum and some singlet state[3] in this low-flux limit.

[2] We are using a number-ket representation where $|n\rangle_{S_x}$ denotes n signal photons in the x-polarized mode of the signal field, etc.

[3] If we let $|0\rangle_T \equiv |1\rangle_{S_x} |0\rangle_{S_y}$, $|1\rangle_T \equiv |0\rangle_{S_x} |1\rangle_{S_y}$, $|0\rangle_R \equiv |1\rangle_{I_x} |0\rangle_{I_y}$, $|1\rangle_R \equiv |0\rangle_{I_x} |1\rangle_{I_y}$, then $|1\rangle_{S_x} |1\rangle_{I_y} |0\rangle_{S_y} |0\rangle_{I_x} - |0\rangle_{S_x} |0\rangle_{I_y} |1\rangle_{S_y} |1\rangle_{I_x} \equiv |0\rangle_T |1\rangle_R - |1\rangle_T |0\rangle_R$, which is the singlet state.

The non-destructive loading verification described in [4] permits the vacuum part to be identified and treated as an erasure in the loading protocol and hence near perfect singlet capture occurs when there is no loss and $\overline{N} << 1$. However, loss is present in any real teleportation system, and it is desirable to increase $\overline{N}$ to compensate for it and maximize throughput. It then follows that higher order terms in (3.2) can no longer be completely neglected, and fidelity-reducing errors can occur. In [2] the simple model that all errors lead to storage of independent random polarizations was used to compute throughput and fidelity. In the next section we will develop a more accurate error model.

Chapter 4

An Error Model for Quantum Communication

A quantum communication system between two parties, allows one party to transmit qubits to the other. There are various ways of achieving this. For instance, a transmitter could send a qubit to a spatially separated receiver by storing the qubit in atomic memory, placing the atom in ultra cold storage and sending the atom in a package by mail to the receiver. In this crude example, we can imagine the possibility of the decoherence of the qubit enroute to the receiver, due to the quantum noise that is a result of interaction with the environment.

The MIT/NU architecture achieves quantum communication by using singlet-state teleportation between a transmitter and receiver. Again, as with all quantum communication systems, we must handle the possibility of the decoherence of the message qubits due to quantum noise. In this chapter we will develop a noisy channel model for our system that will handle such quantum errors.

Two figures of merit that we will be interested in are fidelity (a measure of the accuracy of the communication) and the throughput (the number of qubits we can transmit per second) of the system. We will see that in the MIT/NU architecture there is a tradeoff between these two parameters and we can raise one only at the expense of lowering the other.

4.1 A Bell-diagonal Error Model

In this section we use a cold-cavity approximation to analyze the loading of the memories. We remove the ^{87}Rb from the cavity, making the analysis simpler by avoiding a complex full quantum analysis of the atom-field system.

For the cold-cavity analysis, we need the joint state of four electromagnetic field modes: two in each cavity, one for each polarization. Although each mode can have an arbitrary number of photons in it, the atoms, however, can only absorb one photon. Thus single photon events are accurately treated by this approach. At low enough flux values, higher-order terms can be neglected. Alternatively, as described in Section 4.6, multiple memories can be used to detect multiphoton events allowing them to be treated as erasures.

When we ignore erasures and multiphoton errors, we can deal with a density matrix in the form:

$$\hat{\rho}_{S_x S_y I_x I_y} = \begin{bmatrix} \rho_{00} & \rho_{01} & \rho_{02} & \rho_{03} \\ \rho_{10} & \rho_{11} & \rho_{12} & \rho_{13} \\ \rho_{20} & \rho_{21} & \rho_{22} & \rho_{23} \\ \rho_{30} & \rho_{31} & \rho_{32} & \rho_{33} \end{bmatrix}, \tag{4.1}$$

where 0,1,2,3 denote the Bell-basis states Ψ^-,Ψ^+,Φ^-,Φ^+. We shall show in Appendix A that this Bell-basis density matrix for the joint state of the transmitter and receiver is diagonal, i.e. $\rho_{ij} = 0$ for $i \neq j$. The diagonal elements of $\hat{\rho}_{S_x S_y I_x I_y}$ are the probabilities that the two memories are loaded with the Bell states:

$$\rho_{00} = \Pr[\Psi^-] \tag{4.2}$$

$$\rho_{11} = \Pr[\Psi^+] \tag{4.3}$$

$$\rho_{22} = \Pr[\Phi^-] \tag{4.4}$$

$$\rho_{33} = \Pr[\Phi^+] \tag{4.5}$$

Note that $\mathrm{tr}(\hat{\rho}_{S_x S_y I_x I_y}) < 1$ here, because we have suppressed the erasure and multiphoton events.

Using the cold-cavity approach, Shapiro [2] has shown that the joint density operator for the signal and idler photon as they reach the cavities takes on the factored form, $\hat{\rho}_{\vec{S}\vec{I}} = \hat{\rho}_{S_xI_y}\hat{\rho}_{S_yI_x}$, where the two-mode density operators on the right-hand side are given by the following anti-normally ordered complex-variable characteristic functions:

$$\begin{aligned} \chi_A^{\hat{\rho}_{S_xI_y}}(\zeta_{S_x},\zeta_{I_y}) &= tr[\hat{\rho}_{S_xI_y}e^{-\zeta_{S_x}^*\hat{a}_{S_x}-\zeta_{I_y}^*\hat{a}_{I_y}}e^{+\zeta_{S_x}\hat{a}_{S_x}^\dagger+\zeta_{I_y}\hat{a}_{I_y}^\dagger}] \\ &= e^{-(1+\bar{n})(|\zeta_{S_x}|^2+|\zeta_{I_y}|^2)+2\tilde{n}Re(\zeta_{S_x}\zeta_{I_y})} \end{aligned} \tag{4.6}$$

$$\begin{aligned} \chi_A^{\hat{\rho}_{S_yI_x}}(\zeta_{S_y},\zeta_{I_x}) &= tr[\hat{\rho}_{S_yI_x}e^{-\zeta_{S_y}^*\hat{a}_{S_y}-\zeta_{I_x}^*\hat{a}_{I_x}}e^{+\zeta_{S_y}\hat{a}_{S_y}^\dagger+\zeta_{I_x}\hat{a}_{I_x}^\dagger}] \\ &= e^{-(1+\bar{n})(|\zeta_{S_y}|^2+|\zeta_{I_x}|^2)-2\tilde{n}Re(\zeta_{S_y}\zeta_{I_x})}, \end{aligned} \tag{4.7}$$

where $\bar{n} \equiv I_- - I_+$ and $\tilde{n} \equiv I_- + I_+$, with $I_\mp \equiv \eta_L\gamma\gamma_c G/\Gamma_c(1\mp G)[(1\mp G)\Gamma+\Gamma_c]$. Here: η_L is the propagation loss, γ is the OPA output coupling rate, γ_c is the memory cavity coupling rate, and Γ_c is the memory cavity linewidth. The inverse relation associated with (4.6) is:

$$\hat{\rho}_{S_xI_y} = \int\frac{d^2\zeta_{S_x}}{\pi}\int\frac{d^2\zeta_{I_y}}{\pi}\chi_A^{\hat{\rho}_{S_xI_y}}(\zeta_{S_x},\zeta_{I_y})e^{-\zeta_{S_x}\hat{a}_{S_x}^\dagger-\zeta_{I_y}\hat{a}_{I_y}^\dagger}e^{+\zeta_{S_x}^*\hat{a}_{S_x}+\zeta_{I_y}^*\hat{a}_{I_y}}; \tag{4.8}$$

a similar inverse relation exists for (4.7).

The probability that the x-polarized signal and y-polarized idler photons are in a joint state $|\psi\rangle_{S_xI_y}$ can be most easily found in the transform domain:

$$\begin{aligned} \Pr(|\psi\rangle_{S_xI_y}) &= {}_{S_xI_y}\langle\psi|\hat{\rho}_{S_xI_y}|\Psi\rangle_{S_xI_y} \\ &= {}_{S_xI_y}\langle\psi|\int\frac{d^2\zeta_{S_x}}{\pi}\int\frac{d^2\zeta_{I_y}}{\pi}\chi_A^{\rho_{S_xI_y}}(\zeta_{S_x},\zeta_{I_y}) \\ &\quad e^{-\zeta_{S_x}\hat{a}_{S_x}^\dagger-\zeta_{I_y}\hat{a}_{I_y}^\dagger}e^{+\zeta_{S_x}^*\hat{a}_{S_x}+\zeta_{I_y}^*\hat{a}_{I_y}}|\psi\rangle_{S_xI_y} \\ &= \int\frac{d^2\zeta_{S_x}}{\pi}\int\frac{d^2\zeta_{I_y}}{\pi}\chi_A^{\rho_{S_xI_y}}(\zeta_{S_x},\zeta_{I_y}) \\ &\quad {}_{S_xI_y}\langle\psi|e^{-\zeta_{S_x}\hat{a}_{S_x}^\dagger-\zeta_{I_y}\hat{a}_{I_y}^\dagger}e^{+\zeta_{S_x}^*\hat{a}_{S_x}+\zeta_{I_y}^*\hat{a}_{I_y}}|\psi\rangle_{S_xI_y} \end{aligned} \tag{4.9}$$

4.2 Effect of Errors on Teleporting a Qubit

In our single-photon error model, errors occur when the transmitter and the receiver end up in a Bell state that is not $|\Psi^-\rangle$. To see what effect these errors have on the teleported state, we write out the joint state of the three particle system corresponding to each Bell state in factored form. For the desired singlet state, we have

$$\begin{aligned} |\psi\rangle_{\mathrm{M}}|\Psi^-\rangle_{\mathrm{TR}} &= \frac{1}{2}|\Psi^-\rangle_{\mathrm{TM}}(a|0\rangle_{\mathrm{R}} + b|1\rangle_{\mathrm{R}}) \\ &+\frac{1}{2}|\Psi^+\rangle_{\mathrm{TM}}(-a|0\rangle_{\mathrm{R}} + b|1\rangle_{\mathrm{R}}) \\ &+\frac{1}{2}|\Phi^-\rangle_{\mathrm{TM}}(+a|1\rangle_{\mathrm{R}} + b|0\rangle_{\mathrm{R}}) \\ &+\frac{1}{2}|\Phi^+\rangle_{\mathrm{TM}}(a|1\rangle_{\mathrm{R}} - b|0\rangle_{\mathrm{R}}), \end{aligned} \tag{4.10}$$

as previously shown. Note that the receiver will perform transformations of its state according to the classical information $|\Psi^-\rangle_{\mathrm{TM}} = 00, |\Psi^+\rangle_{\mathrm{TM}} = 01, |\Phi^-\rangle_{\mathrm{TM}} = 10, |\Phi^+\rangle_{\mathrm{TM}} = 11$, using the rules specified in Eqs. (2.26)-(2.29). However, if the memories had been loaded with $|\Psi^+\rangle_{\mathrm{TR}}$ then we would have that

$$\begin{aligned} |\psi\rangle_{\mathrm{M}}|\Psi^+\rangle_{\mathrm{TR}} &= \frac{1}{2}|\Psi^-\rangle_{\mathrm{TM}}(-a|0\rangle_{\mathrm{R}} + b|1\rangle_{\mathrm{R}}) \\ &+\frac{1}{2}|\Psi^+\rangle_{\mathrm{TM}}(a|0\rangle_{\mathrm{R}} + b|1\rangle_{\mathrm{R}}) \\ &+\frac{1}{2}|\Phi^-\rangle_{\mathrm{TM}}(+a|1\rangle_{\mathrm{R}} - b|0\rangle_{\mathrm{R}}) \\ &+\frac{1}{2}|\Phi^+\rangle_{\mathrm{TM}}(a|1\rangle_{\mathrm{R}} + b|0\rangle_{\mathrm{R}}). \end{aligned} \tag{4.11}$$

If we compare (4.10) to (4.11), we see that there is a phase-flip (a phase-difference of π) between corresponding terms. Thus when we attempt to teleport a qubit in this case, the resulting state on the receiver side will contain a phase-flip error, represented by the Pauli-operator $\hat{\sigma}_z$.

Now suppose that the memories have stored $|\Phi^-\rangle_{\rm TR}$. We find that

$$\begin{aligned}|\psi\rangle_{\rm M}|\Phi^-\rangle_{\rm TR} &= \frac{1}{2}|\Psi^-\rangle_{\rm TM}(a|1\rangle_{\rm R}+b|0\rangle_{\rm R})\\ &+\frac{1}{2}|\Psi^+\rangle_{\rm TM}(-a|1\rangle_{\rm R}+b|0\rangle_{\rm R})\\ &+\frac{1}{2}|\Phi^-\rangle_{\rm TM}(+a|0\rangle_{\rm R}+b|1\rangle_{\rm R})\\ &+\frac{1}{2}|\Phi^+\rangle_{\rm TM}(a|0\rangle_{\rm R}-b|1\rangle_{\rm R}),\end{aligned} \tag{4.12}$$

so that comparing (4.10) to (4.12) we see that there is a bit-flip between corresponding terms. Teleporting a qubit will now result in a bit-flip error, represented by the Pauli-operator $\hat{\sigma}_x$.

Finally, if the memories have stored $|\Phi^+\rangle_{\rm TM}$ we get

$$\begin{aligned}|\psi\rangle_{\rm M}|\Phi^+\rangle_{\rm TR} &= \frac{1}{2}|\Psi^-\rangle_{\rm TM}(-a|1\rangle_{\rm R}+b|0\rangle_{\rm R})\\ &+\frac{1}{2}|\Psi^+\rangle_{\rm TM}(-a|1\rangle_{\rm R}+b|0\rangle_{\rm R})\\ &+\frac{1}{2}|\Phi^-\rangle_{\rm TM}(+a|0\rangle_{\rm R}-b|1\rangle_{\rm R})\\ &+\frac{1}{2}|\Phi^+\rangle_{\rm TM}(a|0\rangle_{\rm R}+b|1\rangle_{\rm R}).\end{aligned} \tag{4.13}$$

Now, comparing (4.10) to (4.13) we see that the each term in (4.13) can be obtained by applying the Pauli-operator $\hat{\sigma}_y$ to the corresponding term in (4.10). So teleporting a qubit will result in both a bit-flip and a phase-flip.

To summarize the results of this section, here are single-photon errors, and their results in terms of the Pauli matrices:

$$\begin{aligned}|\psi\rangle &\xrightarrow{\Pr[\Psi^-]} |\psi\rangle\\ &\xrightarrow{\Pr[\Psi^+]} \hat{\sigma}_z|\psi\rangle\\ &\xrightarrow{\Pr[\Phi^-]} \hat{\sigma}_x|\psi\rangle\\ &\xrightarrow{\Pr[\Phi^+]} \hat{\sigma}_y|\psi\rangle,\end{aligned} \tag{4.14}$$

where, for convenience, we have ignored physically unimportant absolute phase factors. In

the next section, we will calculate the probabilities of these error events.

4.3 Error Probabilities

In this section we will derive closed-form expressions for the error probabilities in our error model. We are interested in the probability of a successful teleportation and the probabilities of the various types of errors. To do this, it is necessary to first find the probabilities for the different loading events: Pr[erasure], Pr[Ψ^-], Pr[Ψ^+], Pr[Φ^-] and Pr[Φ^+].

An erasure occurs when either the signal cavity or the idler cavity has zero photons reaching it. This occurs with the following probability:

$$\begin{aligned} \text{Perasure} = {}& {}_{S_y}\langle 0|_{S_x}\langle 0|\hat{\rho}_{S_xS_y}|0\rangle_{S_x}|0\rangle_{S_y} + {}_{I_y}\langle 0|_{I_x}\langle 0|\hat{\rho}_{I_xI_y}|0\rangle_{I_x}|0\rangle_{I_y} - \\ & {}_{S_y}\langle 0|_{S_x}\langle 0|_{I_y}\langle 0|_{I_x}\langle 0|\hat{\rho}_{S_xI_yI_xI_y}|0\rangle_{S_x}|0\rangle_{S_y}|0\rangle_{I_x}|0\rangle_{I_y}. \end{aligned} \tag{4.15}$$

Because the S_x, I_y polarizations are independent of the S_y, I_x polarizations, the above expression can be simplified to:

$$\begin{aligned} \text{Perasure} &= {}_{S_x}\langle 0|\hat{\rho}_{S_x}|0\rangle_{S_x}{}_{S_y}\langle 0|\hat{\rho}_{S_y}|0\rangle_{S_y} + {}_{I_x}\langle 0|\hat{\rho}_{I_x}|0\rangle_{I_x}{}_{I_y}\langle 0|\hat{\rho}_{I_y}|0\rangle_{I_y} \\ &\quad - {}_{I_y}\langle 0|_{S_x}\langle 0|\hat{\rho}_{S_xI_y}|0\rangle_{S_y}|0\rangle_{I_yI_x}\langle 0|_{S_y}\langle 0|\hat{\rho}_{S_yI_x}|0\rangle_{S_y}|0\rangle_{I_x} \qquad (4.16) \\ &= 2\mathrm{p}_0^2 - \mathrm{p}_{00}^2, \qquad (4.17) \end{aligned}$$

where $\mathrm{p}_0 = {}_{S_x}\langle 0|\hat{\rho}_{S_x}|0\rangle_{S_x}$, $\mathrm{p}_{00} = {}_{I_y}\langle 0|_{S_x}\langle 0|\hat{\rho}_{S_xI_y}|0\rangle_{S_x}|0\rangle_{I_y}$ and we have used the symmetry of characteristic functions (4.7) and (4.6).

Teleportation is successful if the transmitter and receiver end up in the singlet state, $|\Psi^-\rangle = \frac{1}{\sqrt{2}}(|1\rangle_{S_x}|0\rangle_{S_y}|0\rangle_{I_x}|1\rangle_{I_y} - |0\rangle_{S_x}|1\rangle_{S_y}|1\rangle_{I_x}|0\rangle_{I_y})$. This occurs with the following probability:

$$
\begin{aligned}
\Pr[\Psi^-] &= \langle\Psi^-|\hat{\rho}_{S_xS_yI_xI_y}|\Psi^-\rangle \\
&= \frac{1}{2}{}_{I_y}\langle 0|_{S_x}\langle 0|\hat{\rho}_{S_xI_y}|0\rangle_{S_x}|0\rangle_{I_yI_x}\langle 1|_{S_y}\langle 1|\hat{\rho}_{S_yI_x}|1\rangle_{S_y}|1\rangle_{I_x} \\
&\quad +\frac{1}{2}{}_{I_y}\langle 1|_{S_x}\langle 1|\hat{\rho}_{S_xI_y}|1\rangle_{S_x}|1\rangle_{I_yI_x}\langle 0|_{S_y}\langle 0|\hat{\rho}_{S_yI_x}|0\rangle_{S_y}|0\rangle_{I_x} \\
&\quad -\frac{1}{2}{}_{I_y}\langle 0|_{S_x}\langle 0|\hat{\rho}_{S_xI_y}|1\rangle_{S_x}|1\rangle_{I_yI_x}\langle 1|_{S_y}\langle 1|\hat{\rho}_{S_yI_x}|0\rangle_{S_y}|0\rangle_{I_x} \\
&\quad -\frac{1}{2}{}_{I_y}\langle 1|_{S_x}\langle 1|\hat{\rho}_{S_xI_y}|0\rangle_{S_x}|0\rangle_{I_yI_x}\langle 0|_{S_y}\langle 0|\hat{\rho}_{S_yI_x}|1\rangle_{S_y}|1\rangle_{I_x} \qquad (4.18) \\
&= \mathrm{p}_{00}\mathrm{p}_{11} + \mathrm{p}_{\mathrm{cross}}, \qquad (4.19)
\end{aligned}
$$

where $\mathrm{p}_{11} = {}_{I_y}\langle 1|_{S_x}\langle 1|\hat{\rho}_{S_xI_y}|1\rangle_{S_x}|1\rangle_{I_y}$, $\mathrm{p}_{\mathrm{cross}} = |{}_{I_y}\langle 0|_{S_x}\langle 0|\hat{\rho}_{S_xI_y}|1\rangle_{S_x}|1\rangle_{I_y}|^2$, and again the symmetries in (4.6) and (4.7) have been used.

Single-photon errors occur if the transmitter and receiver end up in one of the triplet states. The expression for Ψ^+ is similar to the expression above for Ψ^- with the exception of a negative sign:

$$
\begin{aligned}
\Pr[\Psi^+] &= \langle\Psi^+|\hat{\rho}_{S_xS_yI_xI_y}|\Psi^+\rangle \\
&= \mathrm{p}_{00}\mathrm{p}_{11} - \mathrm{p}_{\mathrm{cross}}. \qquad (4.20)
\end{aligned}
$$

The expression for Φ^- is:

$$
\begin{aligned}
\Pr[\Phi^-] &= \langle\Phi^-|\hat{\rho}_{S_xS_yI_xI_y}|\Phi^-\rangle \\
&= \frac{1}{2}{}_{I_y}\langle 1|_{S_x}\langle 0|\hat{\rho}_{S_xI_y}|0\rangle_{S_x}|1\rangle_{I_yI_x}\langle 0|_{S_y}\langle 1|\hat{\rho}_{S_yI_x}|1\rangle_{S_y}|0\rangle_{I_x} \\
&\quad +\frac{1}{2}{}_{I_y}\langle 0|_{S_x}\langle 1|\hat{\rho}_{S_xI_y}|1\rangle_{S_x}|0\rangle_{I_yI_x}\langle 1|_{S_y}\langle 0|\hat{\rho}_{S_yI_x}|0\rangle_{S_y}|1\rangle_{I_x} \\
&\quad -\frac{1}{2}{}_{I_y}\langle 1|_{S_x}\langle 0|\hat{\rho}_{S_xI_y}|1\rangle_{S_x}|0\rangle_{I_yI_x}\langle 0|_{S_y}\langle 1|\hat{\rho}_{S_yI_x}|0\rangle_{S_y}|1\rangle_{I_x} \\
&\quad -\frac{1}{2}{}_{I_y}\langle 0|_{S_x}\langle 1|\hat{\rho}_{S_xI_y}|0\rangle_{S_x}|1\rangle_{I_yI_x}\langle 1|_{S_y}\langle 0|\hat{\rho}_{S_yI_x}|1\rangle_{S_y}|0\rangle_{I_x} \qquad (4.21) \\
&= \mathrm{p}_{10}^2, \qquad (4.22)
\end{aligned}
$$

where $\mathrm{p}_{10} = |{}_{I_y}\langle 1|_{S_x}\langle 0|\hat{\rho}_{S_xI_y}|0\rangle_{S_x}|1\rangle_{I_y}|^2$, symmetry has been exploited again, and the last equality follows from the fact that ${}_{I_y}\langle 0|_{S_x}\langle 1|\hat{\rho}_{S_xI_y}|0\rangle_{S_y}|1\rangle_{I_y} = {}_{I_y}\langle 1|_{S_x}\langle 0|\hat{\rho}_{S_xI_y}|1\rangle_{S_x}|0\rangle_{I_y} = 0$.

The expression for Φ^+ turns out to be identical to the Φ^- case:

$$\begin{aligned} \Pr[\Phi^+] &= \langle \Phi^+ | \hat{\rho}_{S_x S_y I_x I_y} | \Phi^+ \rangle \\ &= p_{10}^2. \end{aligned} \tag{4.23}$$

These four Bell states probabilities are the diagonal terms in the 4×4 joint density matrix (4.1) of the transmitter and the receiver. There are also off-diagonal terms, but we will now show that these are all zero.

4.3.1 Off-diagonal Terms of the Joint Density Operator

Because density operatators are Hermitian, there are only 6 off-diagonal terms we need to consider: $\langle \Psi^- | \hat{\rho}_{S_x S_y I_x I_y} | \Psi^+ \rangle$, $\langle \Psi^- | \hat{\rho}_{S_x S_y I_x I_y} | \Phi^- \rangle$, $\langle \Psi^- | \hat{\rho}_{S_x S_y I_x I_y} | \Phi^+ \rangle$, $\langle \Psi^+ | \hat{\rho}_{S_x S_y I_x I_y} | \Phi^- \rangle$, $\langle \Psi^+ | \hat{\rho}_{S_x S_y I_x I_y} | \Phi^+ \rangle$, $\langle \Phi^- | \hat{\rho}_{S_x S_y I_x I_y} | \Phi^+ \rangle$. In showing that these are all zero, we will use some results that will be proved later in Appendix A:

$$\begin{aligned} {}_{I_y}\langle 1|_{S_x}\langle 1|\hat{\rho}_{S_x I_y}|1\rangle_{S_x}|0\rangle_{I_y} &= 0 \\ {}_{I_y}\langle 0|_{S_x}\langle 0|\hat{\rho}_{S_x I_y}|1\rangle_{S_x}|0\rangle_{I_y} &= 0 \\ {}_{I_y}\langle 0|_{S_x}\langle 1|\hat{\rho}_{S_x I_y}|0\rangle_{S_x}|1\rangle_{I_y} &= 0 \end{aligned} \tag{4.24}$$

The corresponding terms for $\hat{\rho}_{S_x I_y}$ are also zero. It is now easy to calculate the off-diagonal terms. We have that

$$\begin{aligned} & \langle \Psi^- | \hat{\rho}_{S_x S_y I_x I_y} | \Psi^+ \rangle \\ = \; & \frac{1}{2} {}_{I_y}\langle 1|_{S_x}\langle 1|\hat{\rho}_{S_x I_y}|1\rangle_{S_x}|1\rangle_{I_y} {}_{I_x}\langle 0|_{S_y}\langle 0|\hat{\rho}_{S_y I_x}|0\rangle_{S_y}|0\rangle_{I_x} \\ & -\frac{1}{2} {}_{I_y}\langle 0|_{S_x}\langle 0|\hat{\rho}_{S_x I_y}|0\rangle_{S_x}|0\rangle_{I_y} {}_{I_x}\langle 1|_{S_y}\langle 1|\hat{\rho}_{S_y I_x}|1\rangle_{S_y}|1\rangle_{I_x} \\ + \; & \frac{1}{2} {}_{I_y}\langle 1|_{S_x}\langle 1|\hat{\rho}_{S_x I_y}|0\rangle_{S_x}|0\rangle_{I_y} {}_{I_x}\langle 0|_{S_y}\langle 0|\hat{\rho}_{S_y I_x}|1\rangle_{S_y}|1\rangle_{I_x} \\ & -\frac{1}{2} {}_{I_y}\langle 0|_{S_x}\langle 0|\hat{\rho}_{S_x I_y}|1\rangle_{S_x}|1\rangle_{I_y} {}_{I_x}\langle 1|_{S_y}\langle 1|\hat{\rho}_{S_y I_x}|0\rangle_{S_y}|0\rangle_{I_x} \qquad (4.25) \\ = \; & \frac{1}{2} p_{11} p_{00} - \frac{1}{2} p_{11} p_{00} + \frac{1}{2} p_{\text{cross}} - \frac{1}{2} p_{\text{cross}} \qquad (4.26) \\ = \; & 0, \qquad (4.27) \end{aligned}$$

and

$$
\begin{aligned}
& \langle \Psi^- | \hat{\rho}_{S_x S_y I_x I_y} | \Phi^{\mp} \rangle \\
= \; & \frac{1}{2} {}_{I_y}\langle 1|_{S_x}\langle 1|\hat{\rho}_{S_x I_y}|1\rangle_{S_x}|0\rangle_{I_y I_x}\langle 0|_{S_y}\langle 0|\hat{\rho}_{S_y I_x}|0\rangle_{S_y}|1\rangle_{I_x} \\
\mp \; & \frac{1}{2} {}_{I_y}\langle 1|_{S_x}\langle 1|\hat{\rho}_{S_x I_y}|0\rangle_{S_x}|1\rangle_{I_y I_x}\langle 0|_{S_y}\langle 0|\hat{\rho}_{S_y I_x}|1\rangle_{S_y}|0\rangle_{I_x} \\
& -\frac{1}{2} {}_{I_y}\langle 0|_{S_x}\langle 0|\hat{\rho}_{S_x I_y}|1\rangle_{S_x}|0\rangle_{I_y I_x}\langle 1|_{S_y}\langle 1|\hat{\rho}_{S_y I_x}|0\rangle_{S_y}|1\rangle_{I_x} \\
\pm \; & \frac{1}{2} {}_{I_y}\langle 0|_{S_x}\langle 0|\hat{\rho}_{S_x I_y}|0\rangle_{S_x}|1\rangle_{I_y I_x}\langle 1|_{S_y}\langle 1|\hat{\rho}_{S_y I_x}|1\rangle_{S_y}|0\rangle_{I_x} \qquad (4.28) \\
= \; & 0, \qquad (4.29)
\end{aligned}
$$

where the last equality follows from the fact that all the terms in (4.28) are equal to zero.

Similarly, we find that

$$
\begin{aligned}
& \langle \Psi^+ | \hat{\rho}_{S_x S_y I_x I_y} | \Phi^{\mp} \rangle \\
= \; & \frac{1}{2} {}_{I_y}\langle 1|_{S_x}\langle 1|\hat{\rho}_{S_x I_y}|1\rangle_{S_x}|0\rangle_{I_y I_x}\langle 0|_{S_y}\langle 0|\hat{\rho}_{S_y I_x}|0\rangle_{S_y}|1\rangle_{I_x} \\
\mp \; & \frac{1}{2} {}_{I_y}\langle 1|_{S_x}\langle 1|\hat{\rho}_{S_x I_y}|0\rangle_{S_x}|1\rangle_{I_y I_x}\langle 0|_{S_y}\langle 0|\hat{\rho}_{S_y I_x}|1\rangle_{S_y}|0\rangle_{I_x} \\
& +\frac{1}{2} {}_{I_y}\langle 0|_{S_x}\langle 0|\hat{\rho}_{S_x I_y}|1\rangle_{S_x}|0\rangle_{I_y I_x}\langle 1|_{S_y}\langle 1|\hat{\rho}_{S_y I_x}|0\rangle_{S_y}|1\rangle_{I_x} \\
\mp \; & \frac{1}{2} {}_{I_y}\langle 0|_{S_x}\langle 0|\hat{\rho}_{S_x I_y}|0\rangle_{S_x}|1\rangle_{I_y I_x}\langle 1|_{S_y}\langle 1|\hat{\rho}_{S_y I_x}|1\rangle_{S_y}|0\rangle_{I_x} \qquad (4.30) \\
= \; & 0. \qquad (4.31)
\end{aligned}
$$

Finally, we have that

$$
\begin{aligned}
& \langle \Phi^- | \hat{\rho}_{S_x S_y I_x I_y} | \Phi^+ \rangle \\
= \; & \frac{1}{2} {}_{I_y}\langle 1|_{S_x} \langle 0| \hat{\rho}_{S_x I_y} |1\rangle_{S_x} |0\rangle_{I_y I_x} \langle 0|_{S_y} \langle 1| \hat{\rho}_{S_y I_x} |0\rangle_{S_y} |1\rangle_{I_x} \\
& - \frac{1}{2} {}_{I_y}\langle 0|_{S_x} \langle 1| \hat{\rho}_{S_x I_y} |0\rangle_{S_x} |1\rangle_{I_y I_x} \langle 1|_{S_y} \langle 0| \hat{\rho}_{S_y I_x} |1\rangle_{S_y} |0\rangle_{I_x} \\
& + \frac{1}{2} {}_{I_y}\langle 0|_{S_x} \langle 1| \hat{\rho}_{S_x I_y} |1\rangle_{S_x} |0\rangle_{I_y I_x} \langle 1|_{S_y} \langle 0| \hat{\rho}_{S_y I_x} |0\rangle_{S_y} |1\rangle_{I_x} \\
& - \frac{1}{2} {}_{I_y}\langle 0|_{S_x} \langle 1| \hat{\rho}_{S_x I_y} |1\rangle_{S_x} |0\rangle_{I_y I_x} \langle 1|_{S_y} \langle 0| \hat{\rho}_{S_y I_x} |0\rangle_{S_y} |1\rangle_{I_x} \qquad (4.32) \\
= \; & \frac{1}{2} p_{10}^2 - \frac{1}{2} p_{10}^2 \qquad (4.33) \\
= \; & 0. \qquad (4.34)
\end{aligned}
$$

In Appendix A we show that the terms in (4.24) are zero, and we also calculate p_{00}, p_{10}, p_{11}, and p_{cross}.

4.3.2 Summary of Teleportation Errors

Now we shall summarize the error probabilities in terms of p_{00}, p_{10}, p_{11}, and p_{cross}:

$$
\begin{aligned}
\Pr[\Psi^-] &= p_{00}p_{11} + p_{cross} && (4.35) \\
\Pr[\Psi^+] &= p_{00}p_{11} - p_{cross} && (4.36) \\
&= p_{10}^2 && (4.37) \\
\Pr[\Phi^-] &= p_{10}^2 && (4.38) \\
\Pr[\Phi^+] &= p_{10}^2, && (4.39)
\end{aligned}
$$

Where in going from (4.36) to (4.37) we have used the results from Appendix A to show that $p_{00}p_{11} - p_{cross} = p_{10}^2$. We obtain the following reduced density operator:

$$
\hat{\rho}_{S_x S_y I_x I_y} = \begin{bmatrix} p_{00}p_{11} + p_{cross} & 0 & 0 & 0 \\ 0 & p_{10}^2 & 0 & 0 \\ 0 & 0 & p_{10}^2 & 0 \\ 0 & 0 & 0 & p_{10}^2 \end{bmatrix}. \qquad (4.40)
$$

Now, since loading protocol described in Section 3.1 allows us to detect and ignore erasures and the method that will be described in Section 4.6 allows us to detect and ignore multiphoton errors, we can eliminate both these events. This means that the only events to consider are the loading of the four Bell states. This gives us the following conditional density operator

$$\hat{\rho}_{S_x S_y I_x I_y} = \frac{1}{p_{00}p_{11} + p_{cross} + 3p_{10}^2} \begin{bmatrix} p_{00}p_{11} + p_{cross} & 0 & 0 & 0 \\ 0 & p_{10}^2 & 0 & 0 \\ 0 & 0 & p_{10}^2 & 0 \\ 0 & 0 & 0 & p_{10}^2 \end{bmatrix}. \tag{4.41}$$

Note that the trace of this density operator is 1 and that it is the density operator of a Ψ^- Werner state with fidelity, $F = \frac{p_{00}p_{11}+p_{cross}}{p_{00}p_{11}+p_{cross}+3p_{10}^2}$.

In terms of teleportation, this means that we have a quantum channel that will transmit a qubit perfectly with probability F and will apply $\hat{\sigma}_x$, $\hat{\sigma}_y$ and $\hat{\sigma}_z$ each with probability $\frac{1-F}{3}$. This is called a *depolarizing channel* whose operation on a quantum state $\hat{\rho}$ can be represented by:

$$\mathcal{E}(\hat{\rho}) = F\hat{\rho} + \frac{(1-F)}{3}(\hat{\sigma}_x\hat{\rho}\hat{\sigma}_x + \hat{\sigma}_y\hat{\rho}\hat{\sigma}_y + \hat{\sigma}_z\hat{\rho}\hat{\sigma}_z) \tag{4.42}$$

4.4 Teleportation Fidelity and Throughput

The two important figures of merit for our quantum teleportation system are teleportation fidelity (a measure of the faithfulness of communication) and the throughput (the achievable rate of communication) of the system. The teleportation fidelity is defined as $F_T = {}_{in}\langle\psi|\hat{\rho}_{out}|\psi\rangle_{in}$, where ψ_{in} is the input state and $\hat{\rho}_{out}$ is the density operator that describes the output state after completing the teleportation protocol. By linearity, we can express this as

$$\begin{aligned} F_T &= p_{success|no\ erasure}F_{success} + p_{error|no\ erasure}F_{error} \\ &= \frac{p_{success}}{p_{success} + p_{error}} + \frac{1}{3}\frac{p_{error}}{p_{success} + p_{error}} \\ &= 1 - \frac{2}{3}\frac{p_{error}}{p_{success} + p_{error}}. \end{aligned} \tag{4.43}$$

In (4.43), F_{success} and F_{error} are the teleportation fidelities for success and error events: $F_{\text{success}} = 1$, $F_{\text{error}} = 1/3$, as shown in Appendix B. Also, $\text{p}_{\text{success}} = \text{p}_{00}\text{p}_{11} + \text{p}_{\text{cross}}$, and $\text{p}_{\text{error}} = 3\text{p}_{10}^2$, are the success and error probabilities.

For a depolarizing channel we can express the teleportation fidelity F_T in terms of F as

$$F_T = F + \frac{1}{3}(1 - F) \tag{4.44}$$

$$= \frac{2}{3}F + \frac{1}{3}. \tag{4.45}$$

We see that that F_T ranges from $\frac{1}{3}$ when $F = 0$ to 1 when $F = 1$.

The throughput of a quantum communication system using the MIT/NU architecture is limited by the rate at which the memories are loaded with singlet states. Suppose we used a large lattice of atomic memories and ran the loading protocol at 500 kHz. Once a memory is loaded with a singlet state, we can use it for teleportation. This means that if we can load memories at a maximum rate of R pairs s^{-1} then the maximum rate of qubit transmission with our system is R qubits s^{-1}. Thus we can define the throughput N_{success} of a quantum communication system using the MIT/NU architecture, as the rate at which memories are loaded successfully:

$$N_{\text{success}} = \text{p}_{\text{success}} R. \tag{4.46}$$

Here R is the memory cycling rate of 500 kHz.

In Figure 4-1 we have plotted the throughput and fidelity of the quantum communication system under the following conditions: OPAs operating at 1% of their oscillation threshold ($G^2 = .01$), 5 dB of excess loss in each path from the source to the memories, 0.2 dB km^{-1} loss in each fiber, $\frac{\Gamma_c}{\Gamma} = 0.5$ ratio of memory-cavity linewidth to source-cavity linewidth and $R = 500$ kHz. We see from this figure that a throughput of over 200 pair s^{-1} is achievable at an end-to-end path length ($2L$) of 50 km with a fidelity in excess of 97%. The behavior of the achievable throughput with path length is identical to that calculated by Shapiro in [2] but a higher fidelity for a given path length is achieved by our single photon error model as we have reduced the probability of error by converting multiphoton errors into erasures.

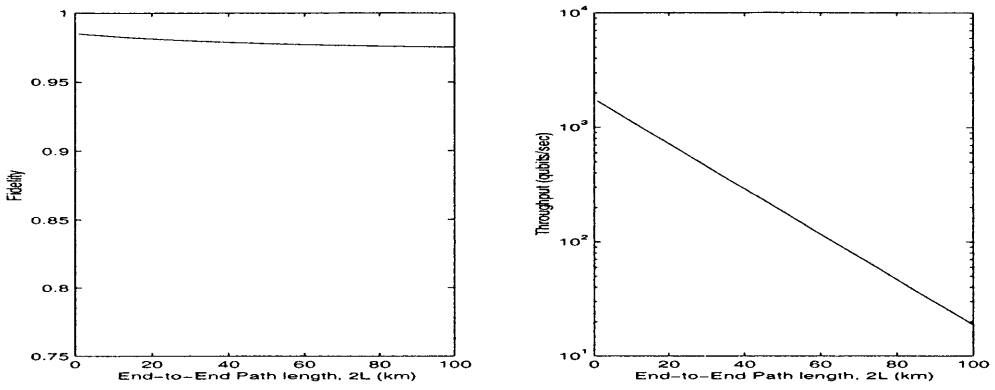

Figure 4-1: Figures of merit for the quantum communication system

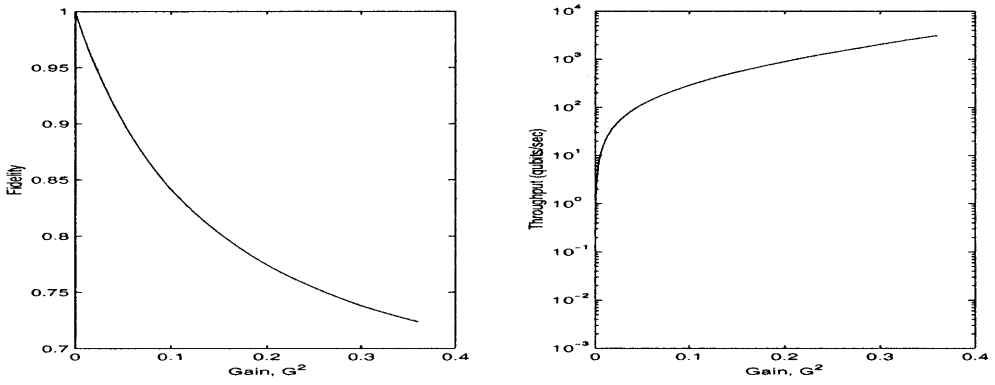

Figure 4-2: Behavior of fidelity and throughput with increasing gain.

4.5 Gain Optimization

To optimize the system for quantum communication, we want to maximize the throughput while maintaining a high fidelity. We can can achieve this by optimizing the gain G^2. More precisely, at any given path length, we would like to find the gain that achieves the maximum throughput - subject to the constraint that fidelity is at least 95%. To do this, we look at plots (Figure 4-2) of fidelity and throughput at a path length of 50 km, against gain values from .01 to .2. As we raise the gain we increase the likelihood of loading events other than the singlet and as a result the fidelity decreases monotonically with gain. On the other hand, the throughput is a monotonically increasing function of gain as raising the gain will reduce the erasure probability. These trends show that we can achieve the maximum throughput subject to our fidelity constraint by adjusting the gain to make fidelity exactly 95%. At 50 km, the optimum gain is 0.024 yielding a throughput of 400 pairs/sec.

In Figure 4-3 we exhibit the achievable throughput after gain optimization. We see that

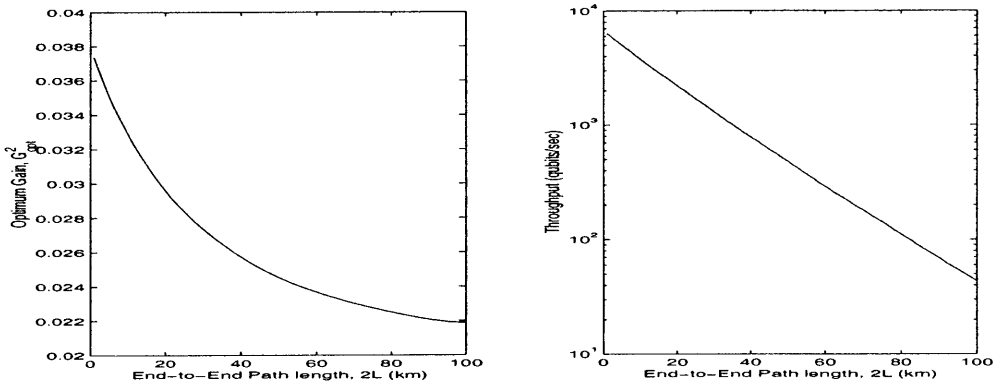

Figure 4-3: Maximum throughput achievable by gain optimization, subject to fidelity being greater than 95%.

at a path length of 50 km we can double the throughput by raising G^2 from 0.01 to 0.024. The cost is a decrease in fidelity from 97.8% to 95%.

4.6 Eliminating Multiphoton Error Events

As the experimental architecture currently stands, restricting our error-model to only single-photon errors is not a good approximation at short path lengths. In fact, as shown in Figure 4-4, at $G^2 = 0.01$, multiphoton errors can only be neglected at long path lengths for which the throughput is very low.

However, we will show in this section that it is possible to reduce the probability of multiphoton error to some value arbitrarily close to zero and improve the single-photon approximation. To do this, we use an array of trapped atoms at either end of the teleportation link for a single memory. Unlike the bank of atomic memories discussed in Section 4.4 where each pair of atoms acted as a memory, this array of atoms will act as a single memory, dedicated to storing the state of a single pair.

In the cold cavity approach, we say that a multiphoton error occurs, when both memories in figure 3-1 load photons, but at least one of the memory cavities loaded two or more photons. The pair of trapped ^{87}Rb atoms in the memories however will each absorb only one photon. In the event of a multi photon error there is a chance that the pair of atoms will absorb photons that are not entangled with one another leading to a teleportation error. The proposed solution is to use beam splitters, and arrays of trapped atoms to detect such events, allowing us to treat them as erasures. Consider the architecture in Figure 4-5, where

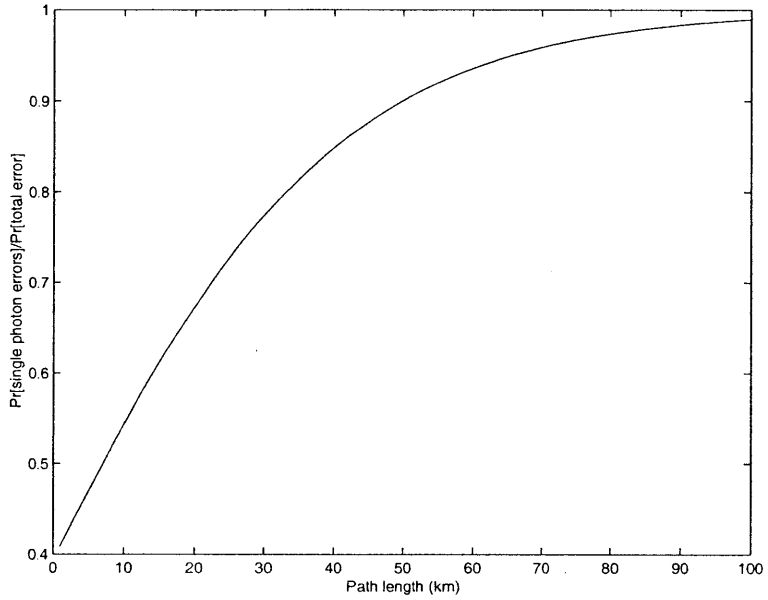

Figure 4-4: A plot of Pr[single-photon error|no erasure]/Pr[total error|no erasure] vs. path-length, L with $\eta_L = 10^{-.02L}$, $\frac{\Gamma_c}{\Gamma} = 0.5$, $\frac{\gamma\gamma_c}{\Gamma\Gamma_c} = 10^{-0.5}$ and $G^2 = .01$. At long path lengths, the likelihood of photons from different pairs reaching the memory cavities is reduced and the single photon model becomes a good approximation. Here, Pr[single-photon error|no erasure] $= \frac{P_{error}}{1-P_{erasure}}$ and Pr[total error|no erasure] $= \frac{1-P_{success}-P_{erasure}}{1-P_{erasure}}$.

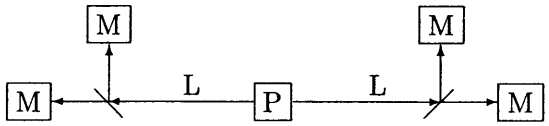

Figure 4-5: Multiphoton error events can be detected using multiple memories. Here we have diagramed 1 level of beam splitter using 2 memories on each side.

instead of having each fiber-optic cable connected directly to a single quantum memory, the optical fibers are connected to lossless 50:50 beam splitters, whose outputs connect to *two* quantum memories (We will later consider the case when there is loss in the memories).

If $n > 1$ photons arrive at one of the beam splitters, the probability that all of them leave through the same output of the beam-splitter is, $\left(\frac{1}{2}\right)^{n-1}$. We can use the non-destructive load verification procedure described in Section 3.1 to count the number of memories that absorb photons. If just one of the photons is split into a different direction and is absorbed into another memory, we will see that more than one memory on either side has been loaded, indicating a multiphoton error. Thus, neglecting any losses in the beam splitters or in the coupling to the memories, the probability of detecting such an event is $1 - \left(\frac{1}{2}\right)^{n-1}$.

If we used k levels of beam splitters and 2^k memories, the probability of detecting a $n > 1$ photon event in a beam becomes $1 - \left(\frac{1}{2}\right)^{k(n-1)}$ in the ideal, lossless case. Note that this value approaches 1 as k increases, showing that it is theoretically possible to eliminate all multiphoton errors with this scheme. In Figure 4-6 we have plotted the number of beam splitters required to reduce the probability of multiphoton error to a small (0.1%) percentage of the probability of single photon error. We see that at longer path lengths our single photon error model becomes a better approximation and fewer beam splitters are required. At an end-to-end path length of 50 km we need 3 beam splitters and 8 atoms per memory.

The analysis in this section assumes the availability of lossless beam splitters. Lossy beam splitters can be treated in the same manner. In fact as shown in Appendix C, for the purposes of this analysis, a photon passing through a series of lossy beam splitters can be modelled as a photon first passing through some fixed loss and then through a series of lossless beam splitters.

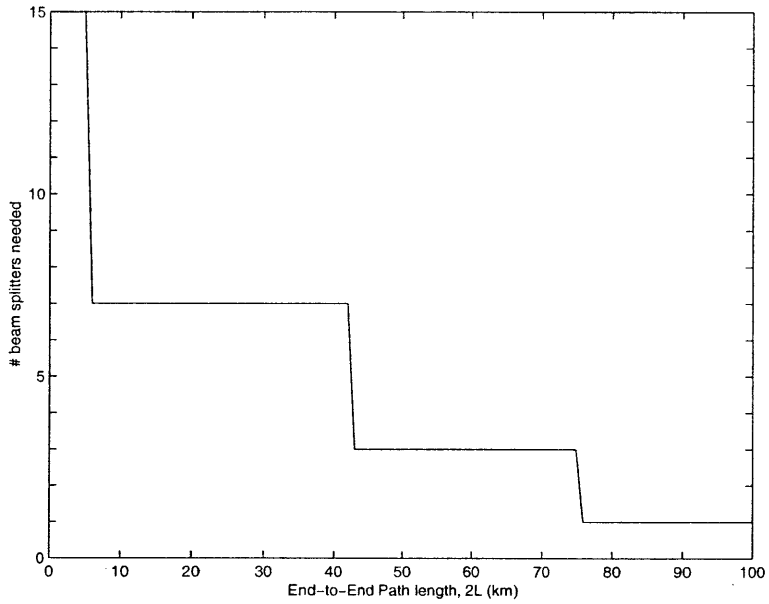

Figure 4-6: The number of levels of beam splitters required to reduce the probability of multiphoton error to 0.1% of the probability of a single photon error at $G^2 = .02$.

Chapter 5

Quantum Error Correcting Codes and Entanglement Purification Protocols

Up to this point, we have developed a model for our quantum communication system as a noisy quantum channel. We see that the entangled pairs are in a Werner state and that attempting to teleport a qubit $|\psi\rangle$ using one of these pairs is equivalent to transmitting $|\psi\rangle$ through a depolarizing channel. We look at the action of this depolarizing channel on $|\psi\rangle$ as the decoherence of $|\psi\rangle$ due to quantum noise. The resulting received state $\hat{\rho}$ is described by the following density operator:

$$\hat{\rho} = F|\psi\rangle\langle\psi| + \frac{(1-F)}{3}(\hat{\sigma}_x|\psi\rangle\langle\psi|\hat{\sigma}_x + \hat{\sigma}_y|\psi\rangle\langle\psi|\hat{\sigma}_y + \hat{\sigma}_z|\psi\rangle\langle\psi|\hat{\sigma}_z) \tag{5.1}$$

where we interpret F as a measure of the severity of the quantum noise. The lower the value of F, he lower the fidelity of quantum communication.

Quantum error correcting codes and entanglement purification protocols are techniques to increase the fidelity of a quantum communication system. We will review examples of such techniques, analyze their application to our communication system and investigate the maximum achievable rate of reliable quantum communication.

5.1 Quantum Error Correcting Codes

An $[[n, k, t]]$ quantum error correcting code is a mapping from k logical qubits to n physical qubits, $k < n$, such that if t or fewer single-qubit errors occur on the physical qubits then we can recover the original logical qubits perfectly. Such a scheme will reduce the probability of error in quantum communication provided that quantum noise is low enough. We will see what this limit for the uncoded fidelity is for the 5-qubit code.

The rate of a quantum error correcting code is defined as $Q = k/n$. This is the number of qubits transmitted per use of the quantum channel.

Quantum error correcting codes can be classified as degenerate or nondegenerate. A nondegenerate code is one for which any two orthogonal errors on a codeword lead to orthogonal states. This allows us to determine the error that has occurred and apply the appropriate transformation to recover the correct state. A degenerate code allows orthogonal errors to map to the same state.

Nondegenerate codes obey a result known as the quantum Hamming bound. For a single qubit system, the Pauli matrices $\hat{\sigma}_x$, $\hat{\sigma}_y$ and $\hat{\sigma}_z$ are three linearly independent transformations that can result from interaction with the environment. For a system of n qubits, the total number of linearly independent transformations on a maximum of t qubits is $\sum_{j=0}^{t} \binom{n}{j} 3^j$.

For a nondegenerate $[[n, k, t]]$ code there are 2^k codewords, so there are $2^k \sum_{j=0}^{t} \binom{n}{j} 3^j$ possible orthogonal states that can result from an interaction with the environment. This gives us a lower bound on the length of the codewords of a nondegenerate quantum code:

$$2^k \sum_{j=0}^{t} \binom{n}{j} 3^j \leq 2^n. \tag{5.2}$$

This is known as the quantum Hamming bound.

A quantum error correcting code need not be nondegenerate. We just require that it allows us to recover the initial state. Degenerate codes can also increase the fidelity of communication. It is suspected, but has yet to be shown, that such codes may be able to pack quantum information more efficiently.

Another bound on quantum codes was derived by Cerf [19]. It is known as the quantum

Singleton bound:

$$n - k \geq 4t \tag{5.3}$$

This is a useful bound because it applies for both degenerate and nondegenerate codes. It also gives us a lower limit on the fidelity of a depolarizing channel below which it is impossible to achieve error-free quantum communication with only quantum error correcting codes.

In the limit of large n, a depolarizing channel of fidelity F will introduce errors to a fraction, $1 - F$, of transmitted qubits. This tells us that a quantum code must correct $t > (1-F)n$ errors. Using the quantum singleton bound, this implies $n-k \geq 4t > 4(1-F)n$. or,

$$\begin{aligned} n - k &> 4n - 4Fn \\ F &> \frac{3}{4} + \frac{k}{4n} \\ F &> \frac{3}{4} \end{aligned} \tag{5.4}$$

We see that, for a depolarizing channel, when $F \leq \frac{3}{4}$ there exists no quantum error correcting code that enables error-free quantum communication. In later sections we will describe techniques for achieving error free communication in the limit of large n for depolarizing channels with $F > \frac{3}{4}$.

Finally we see that for $k = 1$, $t = 1$ the choice of $n = 5$ satisfies both the quantum Hamming bound and the quantum Singleton bound with equality. In the next section, we will analyze the performance of such a quantum error correcting code.

5.1.1 A 5-Qubit Quantum Error Correcting Code

A $[[n = 5, k = 1, t = 1]]$ quantum error correcting code saturates both the quantum Hamming bound and the quantum Singleton bound. In this sense, such codes achieve the best possible performance for $k = 1$.

The first example of a 5-qubit quantum code, discovered by Laflamme [6], used the

following codewords,

$$\begin{aligned} |0\rangle_L &= -|00000\rangle + |01111\rangle - |10011\rangle + |11100\rangle \\ &\quad +|00110\rangle + |01001\rangle + |10101\rangle + |11010\rangle \qquad (5.5) \\ |1\rangle_L &= -|11111\rangle + |10000\rangle + |01100\rangle - |00011\rangle \\ &\quad +|11001\rangle + |10110\rangle - |01010\rangle - |00101\rangle, \qquad (5.6) \end{aligned}$$

where we have ignored the normalization factors. This code uses a relatively simple quantum circuit for the encoding, and the same circuit run backwards for the decoding.

If we try to transmit a qubit $|\psi\rangle$ through a depolarizing channel $\mathcal{E}$ with fidelity F, the fidelity of the received state $\mathcal{E}(|\psi\rangle\langle\psi|)$ is

$$\begin{aligned} \langle\psi|\mathcal{E}(|\psi\rangle\langle\psi|)|\psi\rangle &= F|\langle\psi|\psi\rangle|^2 + \frac{1-F}{3}(|\langle\psi|\hat{\sigma}_x|\psi\rangle|^2 + |\langle\psi|\hat{\sigma}_y|\psi\rangle|^2 + |\langle\psi|\hat{\sigma}_z|\psi\rangle|^2) \\ &= \frac{2F+1}{3}. \qquad (5.7) \end{aligned}$$

For the MIT/NU architecture, the single-photon error channel model is a depolarizing channel with fidelity $F = \mathrm{p_{success}}/(\mathrm{p_{error}} + \mathrm{p_{success}})$, and $\langle\psi|\mathcal{E}(|\psi\rangle\langle\psi|)|\psi\rangle$ is the teleportation fidelity F_T, as can be seen by verifying that $(2F+1)/3 = 1 - 2\mathrm{p_{error}}/3(\mathrm{p_{error}} + \mathrm{p_{success}})$, cf. (4.43).

Application of the 5 qubit code on a depolarizing channel of fidelity F leaves us in a depolarizing channel of fidelity F':

$$\begin{aligned} F' &= \sum_{j=0}^{5} \Pr[j \text{ errors}] F_j \\ &= \sum_{j=0}^{5} \binom{5}{j} (1-F)^j F^{5-j} F_j \qquad (5.8) \\ &= \frac{1}{27}(5 + 20F - 70F^2 + 40F^3 + 160F^4 - 128F^5), \qquad (5.9) \end{aligned}$$

where F_j is the fidelity achieved by the 5 qubit code given that j errors occur on a codeword[1].

[1] In Appendix D, we explain the derivation of F_j's and show that the application of the 5-qubit code leaves us in a depolarizing channel of fidelity F'.

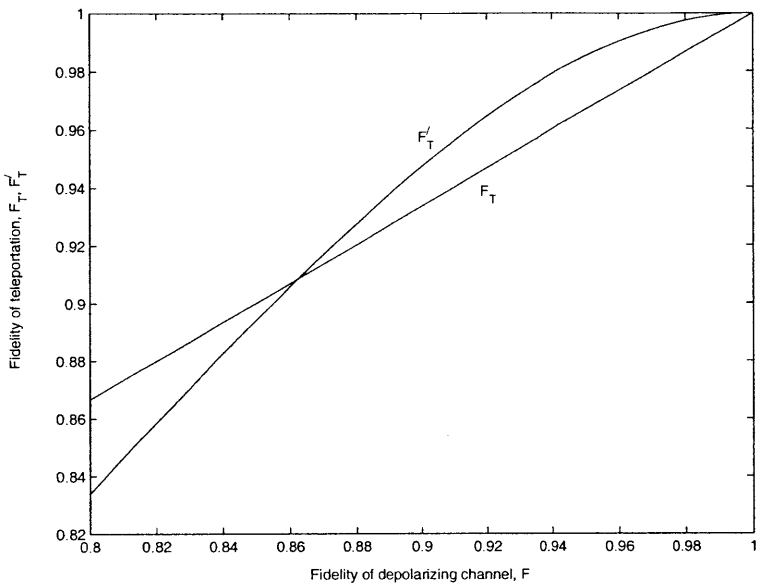

Figure 5-1: Performance of the 5 qubit quantum error correcting code.

The teleportation fidelity after error correction is therefore

$$F'_T = \frac{2F' + 1}{3}. \tag{5.10}$$

In Figure 5-1, we compare the teleportation fidelity of uncoded transmission and 5 qubit code transmission. We see that for a depolarizing channel with $F > 0.8625$, the 5 qubit code provides a fidelity improvement.

We can achieve further improvement in fidelity by encoding the 5 qubit codewords with 25 qubits, i.e., by coding each qubit of the 5 qubit code using a codeword from the same 5 qubit code. The result is a $[[n = 25, k = 1, t = 3]]$ code. However, each time we apply the 5 qubit code we reduce our rate by a factor of 5. In fact, even just 2 applications of the 5 qubit code will require 25 channel uses to transmit a single qubit corresponding to a rate of 0.04. From the point of view of our quantum communication system, if we have a large enough number of entangled pairs, we would like to use quantum codes with larger block lengths that have better distance properties. Several people have discovered such families of good codes [5] [21] that give a positive rate with arbitrarily low probability of error. Alternatively we can use methods known as entanglement purification protocols.

5.2 Entanglement Purification Protocols

An entanglement purification protocol is a series of local operations on n entangled pairs designed to sacrifice $n-k$ of these pairs in order to increase the fidelity of the k remaining pairs. These protocols require classical communication between locations sharing these pairs to coordinate the local operations, i.e. communication between the transmitter and receiver of our teleportation architecture. Protocols that require only one-way communication from the transmitter to the receiver are called one-way protocols and those that require two-way communication are called two-way protocols. In the limit of large n, some protocols can produce a finite number $m < n$ of near-perfect singlets. The yield of an entanglement purification protocol is defined as $D = m/n$ in the limit of large n. Given a large number of entangled pairs and protocol of yield D, we can use the resulting highly pure singlets for teleportation with near zero probability of error. This gives us a method for nearly error free communication at a rate of D qubits per entangled pair.

5.2.1 The One-Way Hashing Protocol

This one-way entanglement purification protocol was introduced by Bennett in [7]. It achieves a finite yield of perfect singlets in the limit of large n. In describing the protocol, we'll assume that n is large and we'll make use of the following two bit notation to represent the Bell states: $|\Psi^-\rangle = 11$, $|\Psi^+\rangle = 01$, $|\Phi^-\rangle = 10$, $|\Phi^+\rangle = 00$.

With this notation, we can describe n independent entangled pairs in a Werner state $\hat{\rho}_F$ as an unknown $2n$ bit string. The hashing protocol is a method that will enable us to determine exactly the values of $2m$ bits in this string and force us to discard $2(n-m)$ bits. Once we know the values of these bits, we can apply unitary transformations to convert the m known Bell states into singlets. Thus the hashing protocol applied to n pairs in a Werner state will yield m perfect singlets. It involves $n-m$ rounds and discards one pair after each round.

In the $k+1$th round, $k = 0, 1, 2, ...n-m-1$ the transmitter and receiver have $n-k$ impure pairs in a Werner state. This can be thought of as an unknown $2(n-k)$ bit string x_k. The transmitter picks and tells the receiver a random $2(n-k)$ bit string s_k called the subset index. The subset index, in turn, determines a random subset of x_k, i.e. the bits of x_k for which corresponding bits in s_k are equal to one. The transmitter and receiver now

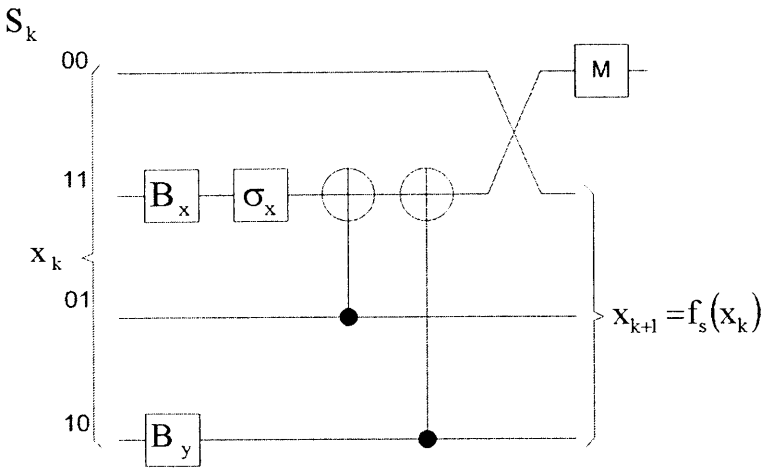

Figure 5-2: We determine the parity of the subset of x_k specified by the index string s_k.

perform a series of unitary operations that collect the parity of this random subset of x_k into a single pair. This procedure, diagrammed in Figure 5-2 is done as follows:

1. The first non-zero bit in s_k is used to select a destination pair in x_k. For instance if we had the following bit sequences:

$$\begin{array}{cccccc} s_k & 00 & 11 & 01 & 10 \\ x_k & 11 & 11 & 10 & 10 \end{array},$$

   we would select the second pair of x_k as the target. Our goal is to collect the parity of the 3rd, 4th, 6th and 6th bits of x_k (the parity of this subset of bits is 1) into the 3rd bit of x_k.

2. In this step we want to collect the subset parity of each pair of bits in x_k into the right bit of that pair. Because pairs in x_k corresponding to 00 pair of bits in s_k don't affect the parity, we will ignore these. For the remaining pairs, look at the corresponding pair of bits in s_k. If a pair of bits in s_k is 01, the corresponding pair of bits in x_k already has the correct parity in the right bit. If a pair of bits in s_k is 10, we swap the left and right bits of the corresponding pair in x_k by applying a $\hat{B}_y$ (Table 2.2). If a pair of bits in s_k is 11, we want to put the parity of the corresponding pair of bits in x_k into the right bit of that pair. This is achieved by applying $\hat{B}_x\hat{\sigma}_x$. Below, we show how this step affects the bit strings in our example.

   Before step 2:

$$\begin{array}{cccccc} s_k & 00 & 11 & 01 & 10 \\ x_k & 11 & 11 & 10 & 10 \end{array},$$

After step 2:

$$\begin{array}{cccccc} s_k & 00 & 11 & 01 & 10 \\ x_k & 11 & 10 & 10 & 01 \end{array}.$$

We see that the first pair of bits in x_k is unaffected because the corresponding pair in s_k is 00. We apply $\hat{B}_x\hat{\sigma_x}$ to the second pair in x_k because the corresponding pair in s_k is 11 (Note that the effect of $\hat{B}_x\hat{\sigma_x}$ is to replace the second bit of the pair with the parity of the pair while leaving the first bit affected). The third pair of bits in x_k is unaffected because the corresponding pair in s_k is 01. We swap the fourth pair of bits in x_k because the corresponding pair in s_k is 10.

3. Now we BXOR all the pairs except the ones corresponding to 00 into the target destination. This will achieve the desired result of collecting the parity of the pairs into the destination. For our example, the resulting x_k is:

$$\begin{array}{cccccc} s_k & 00 & 11 & 01 & 10 \\ x_k & 11 & 11 & 00 & 11 \end{array}.$$

We see that the desired subset parity, 1, has been collected into the right bit of the target (second) pair.

Once the parity of this random subset of x_k has been collected in the target pair, the transmitter and receiver measure $\hat{\sigma}_z$ to determine the subset parity and discard this pair. The remaining unmeasured pairs are in Bell-states characterized by a $2(n-k)-2$ bit string $f_s(x_k)$ that is determined by x_k and s_k.

Bennett shows that under this procedure, in the limit of large n, we will be able to determine the Bell states of m pairs with high probability. His proof is based on the fact that the initial sequence, x_0 consists of n independent and identically distributed random variables and that the typical set for x_0, $\mathcal{L}_\delta^{(n)}$, contains approximately $2^{nS(\hat{\rho}_W)}$[15] likely strings, where $S(\hat{\rho}_W)$ is the von Neumann entropy of the Werner state. These strings are the initial candidates for the true x_0. After every round of the protocol, the determined random subset parity is used to eliminate approximately half of the strings in $\mathcal{L}_\delta^{(n)}$. He

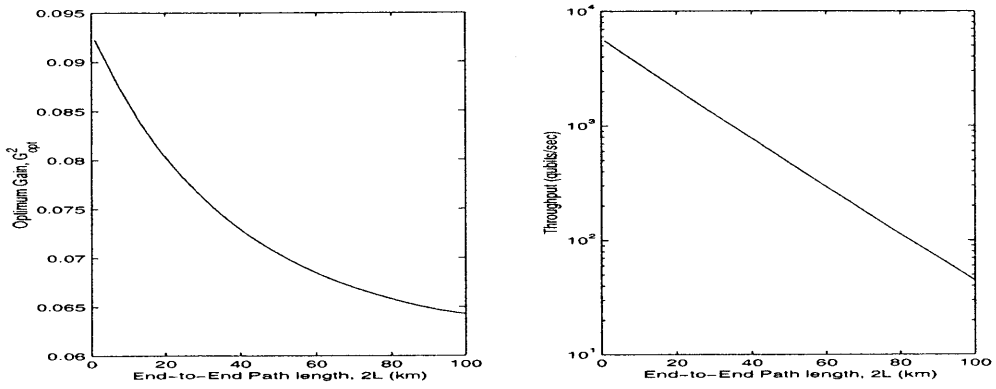

Figure 5-3: Maximum throughput achievable after gain optimization with near perfect fidelity using the hashing protocol.

shows that if we choose $m/n = 1 - S(\hat{\rho}_W)$, then after $n - m$ rounds, we determine true Bell states of the m remaining pairs with high probability.

In the limit of large n this gives us a yield $D_H = m/n$ of

$$D_H = \frac{m}{n} = 1 - S(\hat{\rho}_W). \tag{5.11}$$

For a Werner state, this is

$$D_H = 1 + F\log_2 F + (1-F)\log_2[(1-F)/3]. \tag{5.12}$$

This means that the hashing protocol gives a positive yield of pure singlets for Werner states with $F \geq 0.811$.

In Section 4.5 we showed that the MIT/NU architecture is capable of achieving a throughput of 500 qubits s^{-1} with a fidelity of 95% at an end-to-end path length of 50 km. If we apply the hashing protocol on large blocks of entangled pairs we can distill out a yield $D_H = 0.634$ of near perfect singlets allowing us to teleport qubits with near perfect fidelity. Our throughput is reduced to $D_H N_{\text{success}}$ which is approximately 300 qubits s^{-1}.

We can now optimize the gain of our system to achieve the maximum throughput with near perfect fidelity after applying the hashing protocol. In Figure 5-3 we have plotted the gain-optimized achievable throughput of the MIT/NU teleportation architecture. If we compare Figures 5-3 and 4-3 we immediately see the benefit of employing an entanglement purification protocol. We are able to achieve near perfect fidelity while maintaining our throughput at 50 km after gain optimization at approximately 500 pairs s^{-1}. This is because

the hashing method allows us to use a higher gain at a given path length which increases the success probability for memory loading.

5.2.2 The Recurrence Protocol

The hashing protocol only works on Werner states with $F \geq 0.811$ and in fact no known one-way protocol works unless $F \geq 0.809$ [20]. To purify Werner states with lower fidelities we must use two-way entanglement purification protocols. The recurrence method, first presented by Bennett in [16], is an example of such a two-way protocol. We will review the protocol and describe how it can be used to increase the fidelity of Werner states with $F > 0.5$.

We'll make use of the same two-bit notation for the Bell states as we did in the description of the hashing protocol. The transmitter and receiver share n pairs in a Werner state with $F > 0.5$. One iteration of the protocol proceeds as follows:

1. Apply a $\hat{\sigma_y}$ rotation to convert the Ψ^- Werner state to a Φ^+ Werner state:

$$W_F = F|\Phi^+\rangle\langle\Phi^+| + \frac{1-F}{3}\left(|\Psi^-\rangle\langle\Psi^-| + |\Psi^+\rangle\langle\Psi^+| + |\Phi^-\rangle\langle\Phi^-|\right). \tag{5.13}$$

   The result is a classical mixture of Bell states with probabilities: $q_{00} = F$, $q_{01} = q_{10} = q_{11} = (1-F)/3$.

2. Divide the n pairs into groups of two, and perform CNOT operations on each of these $n/2$ groups, i.e. the transmitter applies a CNOT and the receiver performs a CNOT as diagramed in Figure 5-4.

3. Measure the $\hat{\sigma_z}$ operator on the target pairs from the $n/2$ groups.

4. We keep the source pairs whose target pair $\hat{\sigma_z}$ measurements agree. We discard the source pairs for which the target pair $\hat{\sigma_z}$ measurements disagree. We also discard all the target pairs because we have collapsed their states by measurement.

   If we consider all the possible combinations of source and target states before we perform the CNOTs that will yield agreeing target pair $\hat{\sigma_z}$ measurements after the CNOTs we find that

$$q_{\text{agree}} = q_{00}^2 + q_{01}^2 + q_{10}^2 + q_{11}^2 + 2q_{00}q_{10} + q_{01}q_{11} \tag{5.14}$$

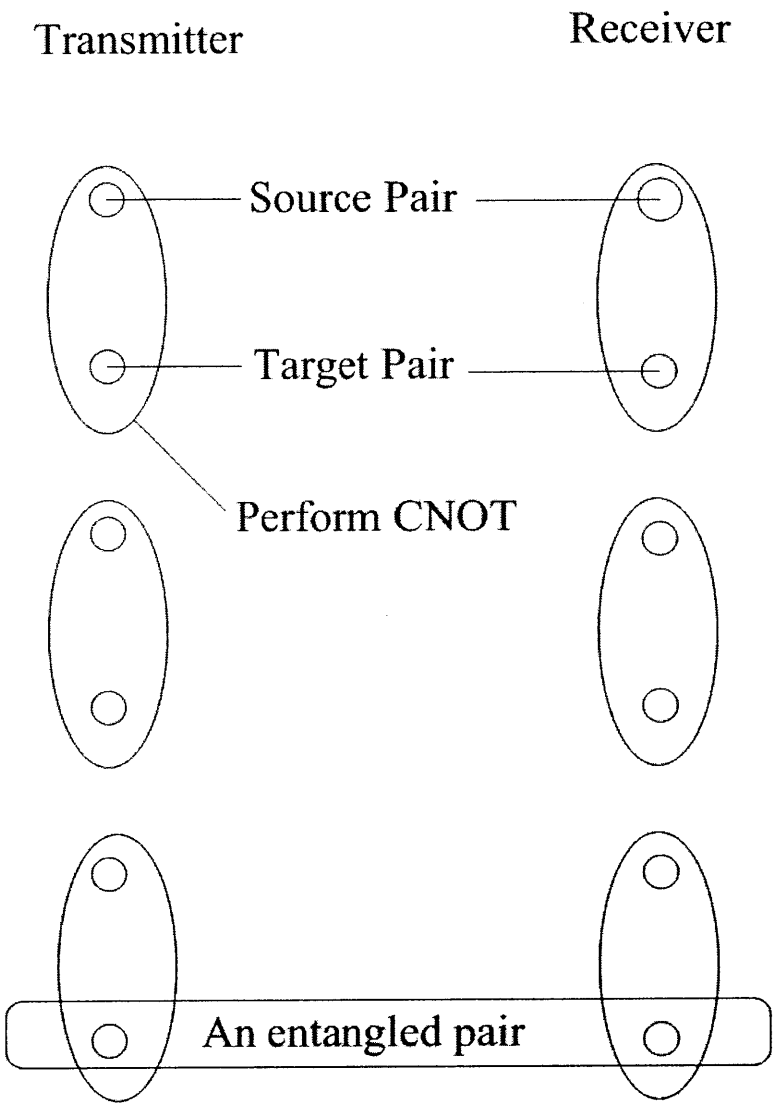

Figure 5-4: A step of the recurrence protocol. We have diagramed six entangled pairs. The transmitter and receiver each perform three CNOTs as shown, then they measure the $\hat{\sigma_z}$ operator on the targets.

where q_{agree} is the probability that the target $\hat{\sigma_z}$ measurements agree.

5. Apply a $\hat{\sigma_y}$ rotation to the remaining pairs swap back the Ψ^- and Φ^+ Werner states.

6. Apply a random bilateral rotation (Table 2.2), equalizing the Ψ^+, Φ^- and Φ^+ states. We are now left with a Ψ^- Werner state of fidelity F' with fewer than half the initial number of pairs.

The fidelity after each iteration F' is greater than the fidelity at the start of the iteration F provided that $F > 0.5$ [16]. Thus the recurrence method is able to increase the fidelity of Werner states that the hashing method cannot. However, half the pairs are measured every round, and some more pairs are discarded at step 4 of the protocol. So although this protocol can be repeated until fidelity is close to 1 (provided we have enough pairs), we see that the the yield in the limit of high fidelity is zero.

A more efficient way to purify Werner states is to use the hashing protocol in combination with this recurrence protocol. We know that the hashing protocol only gives a positive yield for Werner states with $F \geq 0.811$ and the recurrence method can increase the fidelity of Werner states with $F > 0.5$. This means that we can get a positive yield for Werner states with $F > 0.5$ by using the recurrence method to raise the fidelity of the Werner state until it is beneficial to switch over to the hashing protocol, i.e. we switch over as soon as applying the hashing protocol will give a higher yield than will another round of recurrence.

It turns out that for quantum communication over path lengths below 100 km using the MIT/NU teleportation architecture, the use of a combined hashing/recurrence method does not give any advantage over the hashing protocol. This is because using the recurrence protocol in combination with the hashing protocol gives an advantage over the hashing protocol alone only when the initial fidelity is less than about 0.83. At this fidelity, the yield of the combined purification protocol is only 0.1 which means we can do better by raising the gain to increase the fidelity before purification.

However recurrence may be needed if other error effects and imperfections not modelled in this thesis preclude getting an initial fidelity greater than 0.811. In such a situation, we can still achieve reliable quantum communication by using the recurrence protocol to raise the fidelity to the necessary level for the application of the hashing protocol.

5.3 Limits on Quantum Communication

We have shown that by using the hashing entanglement purification protocol, we can achieve reliable quantum communication with the MIT/NU architecture with a throughput of approximately 500 qubits s^{-1} at an end-to-end path length of 50 km. We now need to ask whether we can do better. In this section we'll address the question, "What is the best rate of reliable quantum communication we can achieve with the MIT/NU architecture?"

The answer to this question is the quantum capacity C of the MIT/NU quantum channel, defined to be the maximum number of qubits that can be reliably transmitted with one use of the channel. We can also define two *augmented* quantum capacities, C_1 and C_2 which correspond to the maximum rates of reliable transmission through this channel if we allow unlimited one and two-way classical communication, respectively. Bennett has shown that [7]

$$C = C_1, \tag{5.15}$$

that is to say that unlimited one-way classical communication does not increase the quantum capacity of a quantum channel. It is also clear that

$$C_1 \leq C_2 \tag{5.16}$$

because we can do no worse by allowing classical communication in the other direction. In fact, as we will show later, for a depolarizing channel, such as the MIT/NU system, we do gain capacity by allowing two-way classical communication.

The maximum rate of reliable qubit transmission with our quantum communication system is given by the quantum capacity of a depolarizing channel. Unfortunately, at the time of writing, the computation of quantum capacity for a general input is one of the fundamental unsolved problems in quantum information theory. We will instead, attempt to provide weaker bounds on achievable rates of quantum communication for our system.

In this section, we will make use of an important result shown by Bennett in [7]. He showed that given a one-way entanglement purification protocol of yield D on a Werner state, you can derive a family of quantum error correcting codes that allow reliable qubit transmission through the equivalent depolarizing channel with rate $Q = D$ in the limit of

large block length. Similarly, given a family of quantum error correcting codes that allow reliable qubit transmission through a depolarizing channel at a rate of Q in the limit of large block length, you can derive a one-way entanglement purification protocol of yield $D = Q$ on the equivalent Werner state. Because of this result, any bounds on the performance of quantum error correcting codes apply directly to one-way entanglement purification protocols. Bennett also showed that there is a one-to-one correspondence between bipartite mixed states and noisy quantum channels. We have already seen this in the case of Werner states and depolarizing channels. This means that we can try finding C_1 and C_2 for a quantum channel by looking at the corresponding entanglement purification yields for mixed bipartite states. We will begin by examining three measures for the entanglement of mixed states that will give us guidelines on the ultimate rate of reliable communication achievable with the MIT/NU architecture.

5.3.1 Measures of Mixed State Entanglement

In section 2.2 we gave a quantitative definition of entanglement for pure states. In [7], Bennett has proposed three different measures of entanglement for mixed states that give us bounds on the best yield that entanglement purification protocols can achieve. The first of these is the entanglement of formation of a mixed state, $E(\hat{\rho})$. This is the minimum number of singlet states necessary to create $\hat{\rho}$. We do not know how to compute $E(\hat{\rho})$ for a general mixed state, but Bennett has shown that in the case of a Werner state, $\hat{\rho} = \hat{\rho}_{W_F}$,

$$E(\hat{\rho}_{W_F}) = \begin{cases} H[\frac{1}{2} + \sqrt{F(1-F)}] & \text{for } F \geq \frac{1}{2} \\ 0 & \text{for } F \leq \frac{1}{2} \end{cases} \tag{5.17}$$

where $H(x) = -x\log_2 x - (1-x)\log_2(1-x)$ is the binary entropy function.

The two other measures of entanglement, $D_1(\hat{\rho})$ and $D_2(\hat{\rho})$, are the maximum asymptotic yields of pure singlets that can be prepared from $\hat{\rho}$ with one-way and two-way entanglement purification protocols, respectively. It turns out that these two measures of entanglement, for a given mixed state, are equivalent to the one and two-way augmented capacities of the

corresponding quantum channel [7]:

$$C_1 = D_1(\hat{\rho}) \tag{5.18}$$

$$C_2 = D_2(\hat{\rho}). \tag{5.19}$$

This is because using the singlets distilled from the mixed state for perfect teleportation is equivalent to using the corresponding noisy quantum channel for reliable qubit transmission at a rate equal to the fraction of singlets distilled from the mixed state.

Unfortunately we do not know how to compute D_1 and D_2, even in the case of Bell diagonal states. However it is clear that,

$$E(\hat{\rho}) \geq D_2(\hat{\rho}) \geq D_1(\hat{\rho}), \tag{5.20}$$

where $E(\hat{\rho}) \geq D_2(\hat{\rho})$ because the entanglement of a mixed state cannot be increased by local operations and $D_2(\hat{\rho}) \geq D_1(\hat{\rho})$ because a one-way protocol is just a special case of a two-way protocol. At the moment, there are no explicit results or methods for calculating D_1 and D_2 but we will present upper bounds and lower bounds.

An immediate upper bound on both D_1 and D_2 is given by E. This indicates that the quantum capacity of a depolarizing channel is zero if its fidelity is less that 0.5. An immediate lower bound on D_1 and D_2 is given by the yield of the Hashing protocol, $1 - S(\hat{\rho}_{W_F})$, viz.,

$$D_2 \geq D_1 \geq 1 - S(\hat{\rho}_{W_F}) = 1 + F\log_2 F + (1-F)\log_2[(1-F)/3] \tag{5.21}$$

It turns out that for Werner states, we can find an upper bound on $D_1(\hat{\rho}_{W_F})$ that is tighter than $E(\hat{\rho}_{W_F})$. From the quantum Singleton bound, presented in section 5.1, we know that C_1 for a depolarizing channel is zero if $F < 0.75$. This tells us that D_1 is zero for a Werner state if $F < 0.75$. Now consider a depolarizing channel with $0.75 \leq F \leq 1$. This channel is equivalent to randomly picking between a perfect channel and a $F = 0.75$ depolarizing channel with the probability that we pick the perfect channel equal to $(F-0.75)/(1-0.75)$. D_1 for the Werner state is equal to the capacity C of this composite channel, and the capacity of the composite channel is no greater than $(F-0.75)/(1-0.75)$. So we have,

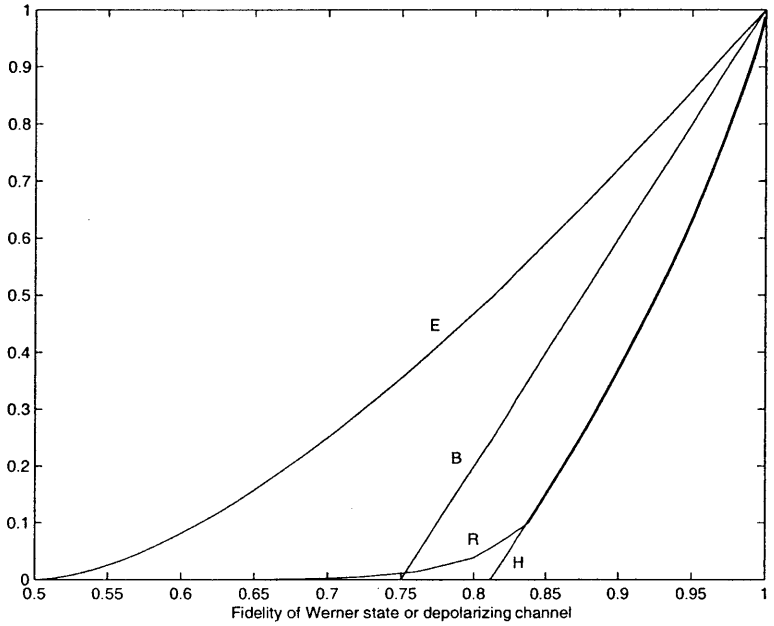

Figure 5-5: Bounds on D_1 and D_2 for Werner states and depolarizing channels. E, the entanglement of formation is an upper bound on D_2. B is the upper bound on D_1 implied by the quantum Singleton bound. R, the yield achieved by an optimal combination of the recurrence protocol and the hashing protocol, is a lower bound for D_2. H, the yield achieved by the hashing protocol alone is a lower bound for D_1.

$$D_1 = C < \frac{F - 0.75}{1 - 0.75} = 4F - 3. \tag{5.22}$$

This gives us a straight line upper bound on D_1.

In Figure 5-5, we summarize the following upper and lower bounds on $C_1 = D_1$ and $C_2 = D_2$:

$$H \leq C_1 \leq B \tag{5.23}$$

$$E \leq C_2 \leq R \tag{5.24}$$

where H is the yield achieved by the hashing protocol, B is the upper bound given in (5.22), E is the entanglement of formation and R is the yield achieved by the optimum combination of recurrence and hashing.

Finally we turn back to the MIT/NU architecture to examine the implications of these bounds on the achievable throughput with near perfect fidelity. Again we plot gain opti-

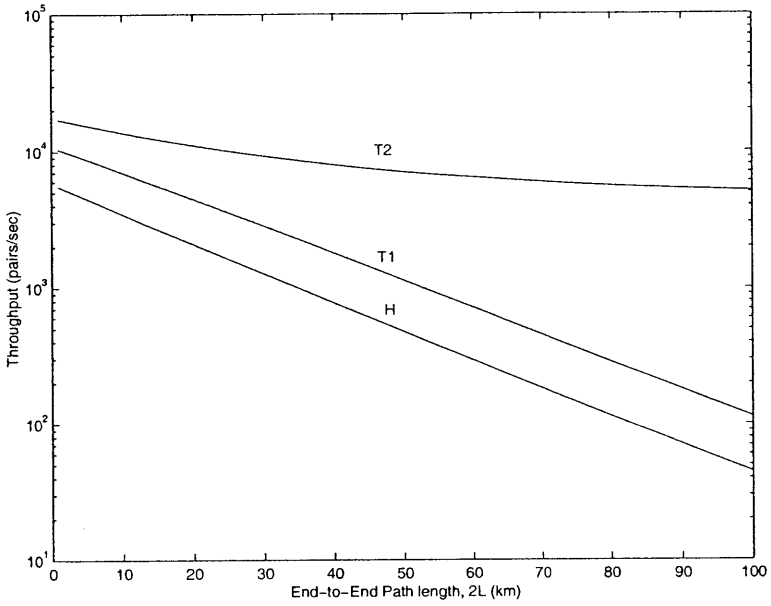

Figure 5-6: Bounds on the achievable throughput with near perfect fidelity. T2 is an upper bound on throughput when we allow two-way classical communication. T1 is an upper bound on throughput when we only allow one-way classical communication. H is the throughput we achieve using the hashing protocol.

mized upper bounds in Figure 5-6. To get an upper bound on the throughput with perfect when we allow two way communication, we assume we have an entanglement purification protocol that achieves a yield $D_2(\hat{\rho}_{W_F}) = E(\hat{\rho}_{W_F})$, we then optimize the gain to achieve the highest throughput with perfect fidelity. Similarly, to obtain an upper bound when we only allow one way communication we assume we have an entanglement purification protocol whose the yield is given by the bound $D_1(\hat{\rho}_{W_F}) = 4F - 3$, for $F > 0.75$. We see that if we only allow one-way classical communication in our error correcting techniques then at an end-to-end path length of 50 km we can at most increase our throughput from 500 to 1200 pairs s^{-1}. If we allow two-way classical communication, at 50 km, we can at most increase our throughput to 7100 pairs s^{-1}.

Chapter 6

Conclusions and Future Work

Driven by advances in the fields of quantum computing and quantum information theory we have developed a model for the MIT/NU long distance quantum teleportation system that allows us to apply techniques from these fields to that system.

We have shown that by using multiple memories to eliminate multiphoton errors, we can model the teleportation of a qubit with the MIT/NU architecture as the transmission of a qubit through a depolarizing channel. This model predicts that we achieve throughputs up to 500 qubits s^{-1} with a fidelity of 95% at an end-to-end path length of 50 km. The model also allowed us to analyze the application of various quantum error correcting codes and entanglement purification protocols to enable communication with near perfect fidelity. In particular, we showed that using the hashing entanglement purification protocol, we can achieve a throughput of of 500 qubits s^{-1} with near-perfect fidelity at 50 km.

We then employed the equivalence of quantum error correcting codes and one-way entanglement purification protocols, and the one-to-one correspondence between depolarizing channels and Werner states to obtain bounds on the best rates of reliable quantum communication achievable with our system. An upper bound for the one-way augmented quantum capacity C_1 of the MIT/NU architecture shows that no more than 1200 pairs s^{-1} can be reliably transmitted at an end-to-end path length of 50 km. Unfortunately the best upper bound for the two-way augmented quantum capacity C_2 of a depolarizing channel that we could find was the entanglement of formation E for the equivalent Werner state. This told us that the achievable rate of reliable quantum communication augmented with two-way classical communication for the MIT/NU architecture is no higher than 7100 pairs s^{-1} at

an end-to-end path length of 50 km. We suspect that this is a very loose bound and the problem of finding a tighter bound on C_2 should be addressed in future work.

Our analysis of the performance of the MIT/NU architecture assumes lossless beam-splitters. However, the actual experimental beam-splitters are imperfect. Although we have described an approach to modelling beam splitter loss (we increase the fixed loss as we increase the number of beam-splitters), in future work, we need to assess the impact of this loss on the performance of the MIT/NU system.

In analyzing the application of entanglement purification protocols to our system we have assumed the availability of arbitrarily large blocks of memories (large n). In reality however, we will only have a finite number of pairs memories in Werner states on which we can run entanglement purification protocols. The consequence is that although we can get very high fidelity by loading a large number of pairs of memories before we run entanglement purification protocols, we cannot achieve perfect fidelity. Thus another issue that needs to be addressed in future work is the performance of *finite block* entanglement purification on the system in terms of fidelity and throughput tradeoffs.

Finally, we note that the communication model presented in this thesis is a first-order approximation to the MIT/NU teleportation system. There are several areas in which the approximation can be improved. We have not modelled possible channel errors such as phase errors due to imperfect polarization compensation in the fiber. There may also be errors resulting from fluctuations in the relative phase and amplitude of the pumps that drive the two OPAs. In addition, errors and imperfections in applying the qubit logic used in teleportation or entanglement purification will reduce the performance of the system. These are only a few of possibly many physical experimental imperfections that should be incorporated into future models.

Appendix A

Moments of $\chi_A^{\hat{\rho}_{S_x I_y}}$ and $\chi_A^{\hat{\rho}_{S_y I_x}}$

To calculate the probabilities of erasure, success and the three single-photon errors, we need the moments of the anti-normally ordered characteristic functions $\chi_A^{\hat{\rho}_{S_x I_y}}$ and $\chi_A^{\hat{\rho}_{S_y I_x}}$. To find these moments, we will follow the derivations sketched by Shapiro in [2]. We see that,

$$\chi_A^{\hat{\rho}_{S_x I_y}} = \frac{\pi^2 f(\zeta)}{(1+\bar{n})^2 - \tilde{n}^2}, \tag{A.1}$$

where $f(\zeta)$ is the classical probability density for a zero-mean, complex-valued Gaussian random vector $\zeta^T = [\zeta_S, \zeta_I]$ whose covariance matrices are

$$\langle \zeta \zeta^\dagger \rangle = \Lambda \equiv \frac{1}{(1+\bar{n})^2 - \tilde{n}^2} \begin{bmatrix} 1+\bar{n} & 0 \\ 0 & 1+\bar{n} \end{bmatrix}, \tag{A.2}$$

and (A.3)

$$\langle \zeta \zeta^T \rangle = \tilde{\Lambda} \equiv \frac{1}{(1+\bar{n})^2 - \tilde{n}^2} \begin{bmatrix} 0 & \tilde{n} \\ \tilde{n} & 0 \end{bmatrix}. \tag{A.4}$$

Similarly,

$$\chi_A^{\hat{\rho}_{S_y I_x}} = \frac{\pi^2 g(\zeta)}{(1+\bar{n})^2 - \tilde{n}^2}, \tag{A.5}$$

where $g(\zeta)$ is the classical probability density for a zero-mean, complex-valued Gaussian

random vector $\zeta^T = [\zeta_S, \zeta_I]$ whose covariance matrices are

$$\langle \zeta \zeta^\dagger \rangle = \Lambda, \tag{A.6}$$

$$\langle \zeta \zeta^T \rangle = -\tilde{\Lambda}. \tag{A.7}$$

With these expressions, we can easily find p_{00}, p_{10}, p_{11} and p_{cross}. In particular, p_{00} follows from the area under $\chi_A^{\hat{\rho}_{S_x I_y}}$,

$$\begin{aligned}
p_{00} &= {}_{I_y}\langle 0|_{S_x}\langle 0|\hat{\rho}_{S_x I_y}|0\rangle_{S_x}|0\rangle_{I_y} \\
&= \int \frac{d^2\zeta_{S_x}}{\pi} \int \frac{d^2\zeta_{I_y}}{\pi} \chi_A^{\hat{\rho}_{S_x I_y}}(\zeta_{S_x}, \zeta_{I_y}) \\
&\quad {}_{I_y}\langle 0|_{S_x}\langle 0|e^{-\zeta_{S_x}\hat{a}^\dagger_{S_x} - \zeta_{I_y}\hat{a}^\dagger_{I_y}} e^{+\zeta^*_{S_x}\hat{a}_{S_x} + \zeta^*_{I_y}\hat{a}_{I_y}}|0\rangle_{S_x}|0\rangle_{Iy} \qquad \text{(A.8)} \\
&= \int \frac{d^2\zeta_{S_x}}{\pi} \int \frac{d^2\zeta_{I_y}}{\pi} \chi_A^{\hat{\rho}_{S_x I_y}}(\zeta_{S_x}, \zeta_{I_y}) \\
&\quad ({}_{I_y}\langle 0|_{S_x}\langle 0|) \cdot (|0\rangle_{S_x}|0\rangle_{Iy}) \\
&= \int \frac{d^2\zeta_{S_x}}{\pi} \int \frac{d^2\zeta_{I_y}}{\pi} \chi_A^{\hat{\rho}_{S_x I_y}}(\zeta_{S_x}, \zeta_{S_y}) \qquad \text{(A.9)} \\
&= \int \frac{d^2\zeta_{S_x}}{\pi} \int \frac{d^2\zeta_{I_y}}{\pi} \frac{\pi^2 f(\zeta)}{(1+\bar{n})^2 - \tilde{n}^2} \qquad \text{(A.10)} \\
&= \frac{1}{(1+\bar{n})^2 - \tilde{n}^2}. \qquad \text{(A.11)}
\end{aligned}$$

We can obtain p_{10} from the second moments of $\chi_A^{\hat{\rho}_{S_x I_y}}$, as follows:

$$\begin{aligned}
p_{10} &= {}_{I_y}\langle 0|_{S_x}\langle 1|\hat{\rho}_{S_x I_y}|1\rangle_{S_x}|0\rangle_{I_y} \\
&= \int \frac{d^2\zeta_{S_x}}{\pi} \int \frac{d^2\zeta_{I_y}}{\pi} [\chi_A^{\hat{\rho}_{S_x I_y}}(\zeta_{S_x}, \zeta_{I_y}) \\
&\quad {}_{I_y}\langle 0|_{S_x}\langle 1|e^{-\zeta_{S_x}\hat{a}^\dagger_{S_x} - \zeta_{I_y}\hat{a}^\dagger_{I_y}} e^{+\zeta^*_{S_x}\hat{a}_{S_x} + \zeta^*_{I_y}\hat{a}_{I_y}}|1\rangle_{S_x}|0\rangle_{Iy}] \qquad \text{(A.12)} \\
&= \int \frac{d^2\zeta_{S_x}}{\pi} \int \frac{d^2\zeta_{I_y}}{\pi} \chi_A^{\hat{\rho}_{S_x I_y}}(\zeta_{S_x}, \zeta_{I_y})[1 - |\zeta_{S_x}|^2] \qquad \text{(A.13)} \\
&= \frac{1}{(1+\bar{n})^2 - \tilde{n}^2}[1 - \langle|\zeta_{S_x}|^2\rangle] \qquad \text{(A.14)} \\
&= \frac{\bar{n}(1+\bar{n}) - \tilde{n}^2}{[(1+\bar{n})^2 - \tilde{n}^2]^2}. \qquad \text{(A.15)}
\end{aligned}$$

We can write p_{11} in terms of p_{00}, p_{10} and a fourth moment of $\chi_A^{\hat{\rho}_{S_x I_y}}$, obtained from the

moment factoring theorem of complex-valued Gaussian random variables:

$$
\begin{aligned}
\mathrm{p}_{11} &= {}_{I_y}\langle 1|_{S_x}\langle 1|\hat{\rho}_{S_xI_y}|1\rangle_{S_x}|1\rangle_{I_y} \\
&= \int \frac{d^2\zeta_{S_x}}{\pi}\int \frac{d^2\zeta_{I_y}}{\pi}[\chi_A^{\hat{\rho}_{S_xI_y}}(\zeta_{S_x},\zeta_{I_y}) \\
&\quad (1-|\zeta_{S_x}|^2-|\zeta_{I_y}|^2+|\zeta_{S_x}|^2|\zeta_{I_y}|^2)] && \text{(A.16)} \\
&= 2\mathrm{p}_{10}-\mathrm{p}_{00}+\int \frac{d^2\zeta_{S_x}}{\pi}\int \frac{d^2\zeta_{I_y}}{\pi}[\chi_A^{\hat{\rho}_{S_xI_y}}(\zeta_{S_x},\zeta_{I_y})|\zeta_{S_x}|^2|\zeta_{I_y}|^2] && \text{(A.17)} \\
&= 2\mathrm{p}_{10}-\mathrm{p}_{00}-\frac{1}{(1+\bar{n})^2-\tilde{n}^2}\langle|\zeta_{S_x}|^2|\zeta_{I_y}|^2\rangle && \text{(A.18)} \\
&= 2\mathrm{p}_{10}-\mathrm{p}_{00} \\
&\quad -\frac{1}{(1+\bar{n})^2-\tilde{n}^2}[\langle|\zeta_{S_x}|^2\rangle\langle|\zeta_{I_y}|^2\rangle+|\langle\zeta_{S_x}\zeta_{I_y}^*\rangle|^2+|\langle\zeta_{S_x}\zeta_{I_x}\rangle|^2] && \text{(A.19)} \\
&= \frac{[\bar{n}(1+\bar{n})-\tilde{n}^2]^2+\tilde{n}^2}{[(1+\bar{n})^2-\tilde{n}^2]^3} && \text{(A.20)}
\end{aligned}
$$

We can calculate $\mathrm{p}_{\mathrm{cross}}$ directly from one of the second moments of $\chi_A^{\hat{\rho}_{S_xI_y}}$:

$$
\begin{aligned}
\mathrm{p}_{\mathrm{cross}} &= |{}_{I_y}\langle 1|_{S_x}\langle 1|\hat{\rho}_{S_xI_y}|0\rangle_{S_x}|0\rangle_{I_y}|^2 \\
&= |\int \frac{d^2\zeta_{S_x}}{\pi}\int \frac{d^2\zeta_{I_y}}{\pi}[\chi_A^{\hat{\rho}_{S_xI_y}}(\zeta_{S_x},\zeta_{I_y})|\zeta_{S_x}\zeta_{I_y}]|^2 && \text{(A.21)} \\
&= \left|\frac{\langle\zeta_{S_x}\zeta_{I_y}\rangle}{(1+\bar{n})^2-\tilde{n}^2}\right|^2 && \text{(A.22)} \\
&= \frac{\tilde{n}^2}{[(1+\bar{n})^2-\tilde{n}^2]^4}. && \text{(A.23)}
\end{aligned}
$$

Finally, we show here that the terms in (4.24) are zero. We have that

$$
\begin{aligned}
&{}_{I_y}\langle 1|_{S_x}\langle 1|\hat{\rho}_{S_xI_y}|1\rangle_{S_x}|0\rangle_{I_y} \\
&= \int \frac{d^2\zeta_{S_x}}{\pi}\int \frac{d^2\zeta_{I_y}}{\pi}[\chi_A^{\hat{\rho}_{S_xI_y}}(\zeta_{S_x},\zeta_{I_y}) \\
&\quad {}_{I_y}\langle 1|_{S_x}\langle 1|e^{-\zeta_{S_x}\hat{a}_{S_x}^\dagger-\zeta_{I_y}\hat{a}_{I_y}^\dagger}e^{+\zeta_{S_x}^*\hat{a}_{S_x}+\zeta_{I_y}^*\hat{a}_{I_y}}|1\rangle_{S_x}|0\rangle_{Iy}], && \text{(A.24)}
\end{aligned}
$$

Series expansions of the exponential terms yields

$$
\begin{aligned}
& e^{+\zeta_{S_x}^* \hat{a}_{S_x} + \zeta_{I_y}^* \hat{a}_{I_y}} |1\rangle_{S_x} |0\rangle_{Iy} \\
= & \sum_{m=0}^{\infty} \frac{(\zeta_{S_x}^* \hat{a}_{S_x} + \zeta_{I_y}^* \hat{a}_{I_y})^m}{m!} |1\rangle_{S_x} |0\rangle_{Iy} && \text{(A.25)} \\
= & |1\rangle_{S_x} |0\rangle_{Iy} + \zeta_{S_x}^* |0\rangle_{S_x} |0\rangle_{Iy}, && \text{(A.26)}
\end{aligned}
$$

and

$$
\begin{aligned}
& {}_{I_y}\langle 1|_{S_x} \langle 1| e^{-\zeta_{S_x} \hat{a}_{S_x}^\dagger - \zeta_{I_y} \hat{a}_{I_y}^\dagger} \\
= & (e^{-\zeta_{S_x}^* \hat{a}_{S_x} - \zeta_{I_y}^* \hat{a}_{I_y}} |1\rangle_{S_x} |0\rangle_{Iy})^\dagger \\
= & (|1\rangle_{S_x} |1\rangle_{I_y} - \zeta_{S_x}^* |0\rangle_{S_x} |1\rangle_{I_y} - \zeta_{I_y}^* |1\rangle_{S_x} |0\rangle_{I_y} + \zeta_{S_x}^* \zeta_{I_y}^* |0\rangle_{S_x} |0\rangle_{I_y})^\dagger. && \text{(A.27)}
\end{aligned}
$$

Taking the inner-product of (A.25) and (A.27) and substituting the result into (A.24) now gives:

$$
\begin{aligned}
& {}_{I_y}\langle 1|_{S_x} \langle 1| \hat{\rho}_{S_x I_y} |1\rangle_{S_x} |0\rangle_{I_y} \\
= & \int \frac{d^2\zeta_{S_x}}{\pi} \int \frac{d^2\zeta_{I_y}}{\pi} \chi_A^{\hat{\rho}_{S_x I_y}}(\zeta_{S_x}, \zeta_{I_y}) [\zeta_{I_y} |\zeta_{S_x}|^2 - \zeta_{I_y}] && \text{(A.28)} \\
= & \frac{1}{(1+\bar{n})^2 - \bar{n}^2} [\langle \zeta_{I_y} |\zeta_{S_x}|^2 - \langle \zeta_{I_x} | \rangle] && \text{(A.29)} \\
= & 0, && \text{(A.30)}
\end{aligned}
$$

where the last equality follows from taking the odd-moments of a zero-mean joint Gaussian distribution.

Via an analogous approach, we obtain:

$$
\begin{aligned}
& {}_{I_y}\langle 0|_{S_x}\langle 0|\hat{\rho}_{S_x I_y}|1\rangle_{S_x}|0\rangle_{I_y} \\
= & \int \frac{d^2\zeta_{S_x}}{\pi}\int \frac{d^2\zeta_{I_y}}{\pi}\chi_A^{\hat{\rho}_{S_x I_y}}(\zeta_{S_x},\zeta_{I_y}) \\
& {}_{I_y}\langle 0|_{S_x}\langle 0|e^{-\zeta_{S_x}\hat{a}^\dagger_{S_x}-\zeta_{I_y}\hat{a}^\dagger_{I_y}}e^{+\zeta^*_{S_x}\hat{a}_{S_x}+\zeta^*_{I_y}\hat{a}_{I_y}}|1\rangle_{S_x}|0\rangle_{Iy} && \text{(A.31)} \\
= & \int \frac{d^2\zeta_{S_x}}{\pi}\int \frac{d^2\zeta_{I_y}}{\pi}\chi_A^{\hat{\rho}_{S_x I_y}}(\zeta_{S_x},\zeta_{I_y}) \\
& ({}_{I_y}\langle 0|_{S_x}\langle 0|)\cdot(|1\rangle_{S_x}|0\rangle_{Iy}+\zeta^*_{S_x}|0\rangle_{S_x}|0\rangle_{Iy}) && \text{(A.32)} \\
= & \int \frac{d^2\zeta_{S_x}}{\pi}\int \frac{d^2\zeta_{I_y}}{\pi}\chi_A^{\hat{\rho}_{S_x I_y}}(\zeta_{S_x},\zeta_{I_y})\zeta^*_{S_x} && \text{(A.33)} \\
= & \frac{\langle\zeta^*_{S_x}\rangle}{(1+\bar{n})^2-\tilde{n}^2} && \text{(A.34)} \\
= & 0. && \text{(A.35)}
\end{aligned}
$$

Finally, we have that

$$
\begin{aligned}
& {}_{I_y}\langle 0|_{S_x}\langle 1|\hat{\rho}_{S_x I_y}|0\rangle_{S_x}|1\rangle_{I_y} \\
= & \int \frac{d^2\zeta_{S_x}}{\pi}\int \frac{d^2\zeta_{I_y}}{\pi}\chi_A^{\hat{\rho}_{S_x I_y}}(\zeta_{S_x},\zeta_{I_y}) \\
& {}_{I_y}\langle 0|_{S_x}\langle 1|e^{-\zeta_{S_x}\hat{a}^\dagger_{S_x}-\zeta_{I_y}\hat{a}^\dagger_{I_y}}e^{+\zeta^*_{S_x}\hat{a}_{S_x}+\zeta^*_{I_y}\hat{a}_{I_y}}|0\rangle_{S_x}|1\rangle_{Iy} && \text{(A.36)} \\
= & \int \frac{d^2\zeta_{S_x}}{\pi}\int \frac{d^2\zeta_{I_y}}{\pi}\chi_A^{\hat{\rho}_{S_x I_y}}(\zeta_{S_x},\zeta_{I_y}) \\
& ({}_{I_y}\langle 0|_{S_x}\langle 1|-\zeta_{S_x I_y}\langle 0|_{S_x}\langle 0|)\cdot(|0\rangle_{S_x}|1\rangle_{Iy}+\zeta^*_{I_y}|0\rangle_{S_x}|0\rangle_{Iy}) \\
= & \int \frac{d^2\zeta_{S_x}}{\pi}\int \frac{d^2\zeta_{I_y}}{\pi}\chi_A^{\hat{\rho}_{S_x I_y}}(\zeta_{S_x},\zeta_{I_y})\zeta_{S_x}\zeta^*_{I_y} && \text{(A.37)} \\
= & \frac{\langle\zeta_{S_x}\zeta^*_{I_y}\rangle}{(1+\bar{n})^2-\tilde{n}^2} && \text{(A.38)} \\
= & 0, && \text{(A.39)}
\end{aligned}
$$

where the final equality can be found from the second moments of $\chi_A^{\hat{\rho}_{S_x I_y}}$.

Appendix B

The Average Fidelity of Pauli Errors

To define the notion of an average fidelity of quantum communication we write a qubit as

$$|\psi\rangle = \alpha|0\rangle + \beta|1\rangle \tag{B.1}$$

$$= \cos\left(\frac{\theta}{2}\right)|0\rangle + e^{i\phi}\sin\left(\frac{\theta}{2}\right)|1\rangle. \tag{B.2}$$

This can be done because $|\alpha|^2 + |\beta|^2 = 1$. The numbers ϕ and θ define a point on the three-dimensional unit sphere known as the Bloch sphere. We can think of a random qubit as being uniformly distributed over this sphere. Keeping this idea in mind, we turn to the issue of finding the average fidelity of quantum communication.

If we send a qubit $|\psi\rangle$ through a quantum channel that applies the identity operator $\hat{I}$ to $|\psi\rangle$ we have an output fidelity of

$$F_{\hat{I}} = |\langle\psi|\hat{I}|\psi\rangle|^2 \tag{B.3}$$

$$= ||\alpha|^2 + |\beta|^2|^2 \tag{B.4}$$

$$= 1. \tag{B.5}$$

If the channel applies the Pauli operator $\hat{\sigma}_x$ to $|\psi\rangle$, the fidelity of the system is

$$\begin{aligned} F_{\hat{\sigma}_x} &= |\langle\psi|\hat{\sigma}_x|\psi\rangle|^2 && \text{(B.6)} \\ &= |\alpha^*\beta + \alpha\beta^*|^2 && \text{(B.7)} \\ &= 4\mathrm{Re}^2(\alpha^*\beta). && \text{(B.8)} \end{aligned}$$

This is the fidelity for a given qubit. To find the average fidelity for a random qubit, we can use our picture of the qubit uniformly distributed over the Bloch sphere:

$$\begin{aligned} \bar{F}_{\hat{\sigma}_x} &= \frac{1}{4\pi}\int_0^{\pi}\int_0^{2\pi} |\langle\psi|\hat{\sigma}_x|\psi\rangle|^2 \sin\theta d\theta d\phi && \text{(B.9)} \\ &= \frac{1}{4\pi}\int_0^{\pi}\int_0^{2\pi} 4\mathrm{Re}^2(\alpha^*\beta)\sin\theta d\theta d\phi && \text{(B.10)} \\ &= \frac{1}{4\pi}\int_0^{\pi}\int_0^{2\pi} \sin^3\theta\cos^2\phi d\theta d\phi && \text{(B.11)} \\ &= \frac{1}{3}. && \text{(B.12)} \end{aligned}$$

Using a similar approach we find the average fidelity of $\hat{\sigma}_y$ and $\hat{\sigma}_z$ obtaining the following results:

$$\begin{aligned} \bar{F}_{\hat{\sigma}_y} &= \frac{1}{4\pi}\int_0^{\pi}\int_0^{2\pi} |\langle\psi|\hat{\sigma}_y|\psi\rangle|^2 d\theta d\phi && \text{(B.13)} \\ &= \frac{1}{3}, && \text{(B.14)} \\ \bar{F}_{\hat{\sigma}_z} &= \frac{1}{4\pi}\int_0^{\pi}\int_0^{2\pi} |\langle\psi|\hat{\sigma}_z|\psi\rangle|^2 d\theta d\phi && \text{(B.15)} \\ &= \frac{1}{3}. && \text{(B.16)} \end{aligned}$$

Appendix C

Modelling Lossy Beam Splitters

In section 4.6 we assumed the availability of lossless beam splitters. We'll now show that a photon passing through a lossy symmetric beam splitter can be modelled as a photon first passing through some fixed loss and then through a lossless beam splitter. We will not treat the case of asymmetric loss at the output ports.

First note that a lossless 50:50 beam splitter diagrammed in Figure C-1 has the following input/output annihilation operator relationship for one mode of the electromagnetic field:

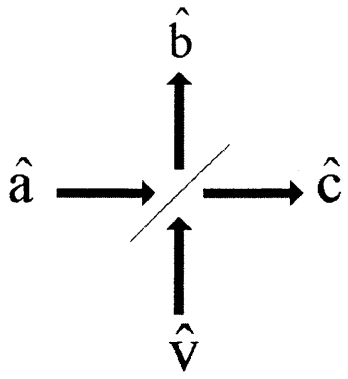

Figure C-1: Lossless 50:50 beam splitter.

$$\hat{b} = \frac{1}{\sqrt{2}}\hat{a} - \frac{1}{\sqrt{2}}\hat{v} \tag{C.1}$$

$$\hat{c} = \frac{1}{\sqrt{2}}\hat{a} + \frac{1}{\sqrt{2}}\hat{v} \tag{C.2}$$

For our purposes the $\hat{a}$ mode will be excited and the $\hat{v}$ mode will be in the vacuum state. Quantum loss on the $\hat{a}$ mode at the input to the 50:50 beam splitter can then be modelled by placing a lossless ϵ-beam splitter in front of the $\hat{a}$ input port of a lossless beam splitter as shown in Figure C-2. In this case we have the following annihilation operator input/output relationship:

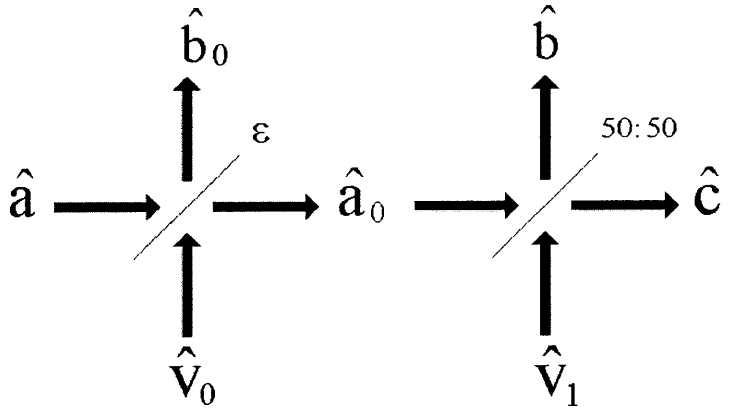

Figure C-2: Model for a 50:50 beam splitter with input loss on the $\hat{a}$ mode: a lossless ϵ-beam splitter followed by a lossless 50:50 beam splitter.

$$\hat{a}_0 = \sqrt{\epsilon}\hat{a} + \sqrt{1-\epsilon}\hat{v}_0 \tag{C.3}$$

$$\hat{b} = \sqrt{\frac{\epsilon}{2}}\hat{a} + \sqrt{\frac{1-\epsilon}{2}}\hat{v}_0 - \frac{1}{\sqrt{2}}\hat{v}_1 \tag{C.4}$$

$$\hat{c} = \sqrt{\frac{\epsilon}{2}}\hat{a} + \sqrt{\frac{1-\epsilon}{2}}\hat{v}_0 + \frac{1}{\sqrt{2}}\hat{v}_1, \tag{C.5}$$

and $\hat{v}_0$, $\hat{v}_1$ are both in vacuum states. The antinormally ordered characteristic function of the joint density operator at the output ports in Figure C-2 is,

$$\chi_A^{\hat{\rho}_{\hat{b}\hat{c}}}(\zeta_b, \zeta_c, \zeta_b^*, \zeta_c^*) = \mathrm{tr}\left[\hat{\rho}_{\hat{b}\hat{c}} e^{-\zeta_b^*\hat{b} - \zeta_c^*\hat{c}} e^{\zeta_b\hat{b}^\dagger + \zeta_c\hat{c}^\dagger}\right] \tag{C.6}$$

$$= \chi_A^{\hat{\rho}_{\hat{a}}}\left(\sqrt{\frac{\epsilon}{2}}(\zeta_b^* + \zeta_c^*), \sqrt{\frac{\epsilon}{2}}(\zeta_b + \zeta_c)\right) e^{-\left(\frac{1-\epsilon}{2}\right)|\zeta_b+\zeta_c|^2} e^{-\frac{1}{2}|\zeta_b-\zeta_c|^2}. \tag{C.7}$$

Now let us consider the case of symmetric loss at the output ports of a 50:50 beam splitter shown in Figure C-1. This situation can be modelled by placing a lossless ϵ-beam split-

ter at each output port, as diagramed in Figure C-3, giving the following input/output relationships:

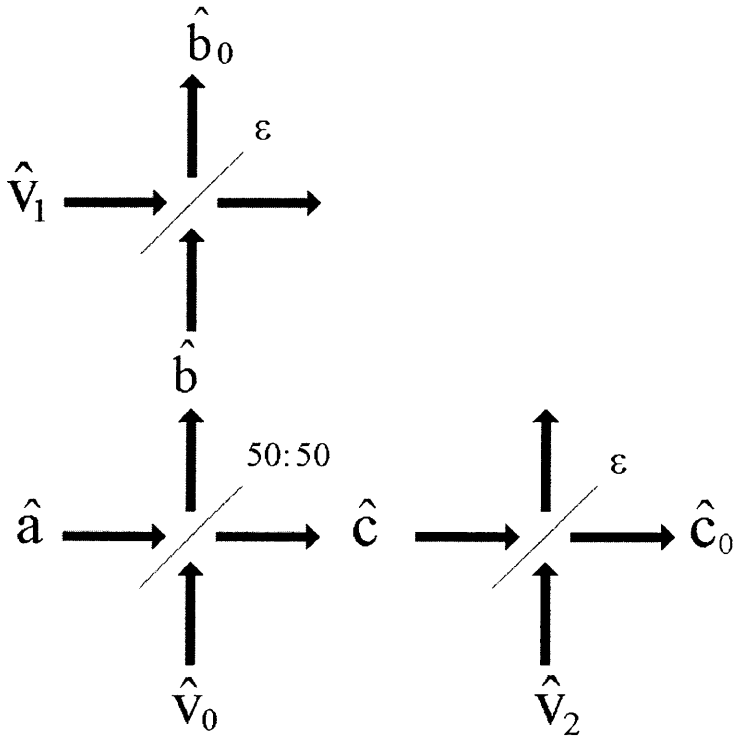

Figure C-3: Model for a 50:50 beam splitter with symmetric output loss: a lossless 50:50 beam splitter with lossless ϵ-beam splitters in each output port.

$$\hat{b} = \frac{\hat{a} - \hat{v}_0}{\sqrt{2}} \tag{C.8}$$

$$\hat{c} = \frac{\hat{a} + \hat{v}_0}{\sqrt{2}} \tag{C.9}$$

$$\hat{b}_0 = \sqrt{\epsilon}\hat{b} + \sqrt{1-\epsilon}\hat{v}_1 \tag{C.10}$$

$$= \sqrt{\frac{\epsilon}{2}}\hat{a} - \sqrt{\frac{\epsilon}{2}}\hat{v}_0 + \sqrt{1-\epsilon}\hat{v}_1 \tag{C.11}$$

$$\hat{c}_0 = \sqrt{\epsilon}\hat{c} + \sqrt{1-\epsilon}\hat{v}_2 \tag{C.12}$$

$$= \sqrt{\frac{\epsilon}{2}}\hat{a} + \sqrt{\frac{\epsilon}{2}}\hat{v}_0 + \sqrt{1-\epsilon}\hat{v}_2, \tag{C.13}$$

where $\hat{v}_0$, $\hat{v}_1$ and $\hat{v}_2$ are in vacuum states. This gives us the antinormally ordered characteristic function of the joint density operator at the output ports of a beam splitter with

symmetric output loss:

$$\chi_A^{\hat{\rho}_{\hat{b}_0\hat{c}_0}}(\zeta_b,\zeta_c,\zeta_b^*,\zeta_c^*) = \mathrm{tr}\left[\hat{\rho}_{\hat{b}_0\hat{c}_0} e^{-\zeta_b^*\hat{b}_0-\zeta_c^*\hat{c}_0} e^{\zeta_b\hat{b}_0^\dagger+\zeta_c\hat{c}_0^\dagger}\right] \tag{C.14}$$

$$= \chi_A^{\hat{\rho}_{\hat{a}}}\left(\sqrt{\frac{\epsilon}{2}}(\zeta_b^*+\zeta_c^*), \sqrt{\frac{\epsilon}{2}}(\zeta_b+\zeta_c)\right) e^{-\frac{\epsilon}{2}|\zeta_b+\zeta_c|^2} e^{-(1-\epsilon)|\zeta_b|^2} e^{-(1-\epsilon)|\zeta_c|^2} \tag{C.15}$$

$$= \chi_A^{\hat{\rho}_{\hat{a}}}\left(\sqrt{\frac{\epsilon}{2}}(\zeta_b^*+\zeta_c^*), \sqrt{\frac{\epsilon}{2}}(\zeta_b+\zeta_c)\right) e^{-\left(\frac{1-\epsilon}{2}\right)|\zeta_b+\zeta_c|^2} e^{-\frac{1}{2}|\zeta_b-\zeta_c|^2}, \tag{C.16}$$

which is identical to (C.7). Thus we see that applying a non-vacuum state to one input of a beam splitter with ϵ-loss at each of the output ports and zero loss at the input is equivalent to applying that same non-vacuum state to one input of a beam splitter with ϵ-loss at the input port and zero loss at the output ports. This means that we can examine the impact of beam-splitter loss on our scheme for eliminating multiphoton errors by assuming lossless beam splitters and appropriately increasing the fixed loss that is encountered before the beam splitter array.

Appendix D

Fidelity of the 5-qubit Quantum Error Correcting Code

The analysis of the 5-qubit Quantum Error Correcting Code presented in Section 5.1.1 was done by simulation of Laflamme's 5-qubit code [6]. The system of 5 qubits is represented as a $2^5 = 32$ column vector whose elements are the projections of the state onto the computational basis vectors $|00000\rangle$, $|00001\rangle$ $|00010\rangle$, etc. The encoding $\hat{C}$ and decoding $\hat{C}^{-1}$ circuits are represented by 32 by 32 unitary matrices. The noise is represented by 1024 possible different unitary matrices, $\hat{E}_0, \hat{E}_1, ...\hat{E}_{1023}$, placed after the encoder and before the decoder. [Because there are 4 operations ($\hat{I}$, $\hat{\sigma_x}$, $\hat{\sigma_y}$ and $\hat{\sigma_z}$) that can occur on each of the 5 qubits, there are 1024 different errors.]

We measured the error syndrome on $\hat{C}^{-1}\hat{E}_i\hat{C}|\psi\rangle$ for $i = 0, 1, ...1023$ and performed the appropriate transformation to determine the output state. We found that all the errors correspond to one of $\hat{I}$, $\hat{\sigma_x}$, $\hat{\sigma_y}$ and $\hat{\sigma_z}$. And these errors are distributed as in Table D.1. We see two things from Table D.1. The first is that the number of correct decodings

# Qubits affected	# Different errors	$\hat{I}$	$\hat{\sigma}_x$	$\hat{\sigma}_y$	$\hat{\sigma}_z$
0	1	1	0	0	0
1	15	15	0	0	0
2	90	0	30	30	30
3	270	60	70	70	70
4	405	135	90	90	90
5	243	45	66	66	66

Table D.1: Distribution of errors suffered by a qubit coded with the 5 qubit code.

and Pauli errors add up exactly to the total number of different errors. This means that correct decodings and Pauli errors are the only possible decoding outcomes. This is because measuring the error syndrome collapses the state of the decoded qubit into either $|\psi\rangle_{\text{in}}$, $\hat{\sigma}_x|\psi\rangle_{\text{in}}$, $\hat{\sigma}_y|\psi\rangle_{\text{in}}$ or $\hat{\sigma}_z|\psi\rangle_{\text{in}}$. We also see that for each row in the table, all three Pauli errors occur with equal likelihood. This means that application of the 5 qubit code to a depolarizing channel of fidelity F will leave us in another depolarizing channel of fidelity F' (where F' is found in Section 5.1.1).

For the purposes of Section 5.1.1 the fidelity given j errors occur F_j can be found from Table D.1.

$$F_0 = 1 \tag{D.1}$$

$$F_1 = 1 \tag{D.2}$$

$$F_2 = 0 \tag{D.3}$$

$$F_3 = \frac{2}{9} \tag{D.4}$$

$$F_4 = \frac{1}{3} \tag{D.5}$$

$$F_5 = \frac{5}{27}. \tag{D.6}$$

Bibliography

[1] C.H. Bennett, G. Brassard, C. Crépeau, R. Jozsa, A. Peres and W.K. Wootters, "Teleporting an unknown quantum state via dual classical and Einstein-Podolsky-Rosen channels," Phys. Rev. Letters **70**, 1895-1899 (1993).

[2] J.H. Shapiro, "Architectures for long-distance quantum teleportation," to appear in New J. Phys.

[3] J.H. Shapiro and N.C. Wong, "An ultrabright narrowband source of polarization-entangled photon pairs," J. Opt. B: Quantum Semiclass. Opt. **2**, L1-L4 (2000).

[4] S. Lloyd, M.S. Shahriar, J.H. Shapiro and P.R. Hemmer, "Long distance, unconditional teleportation of atomic states via complete Bell state measurements," Phys. Rev. Letters **87**, 167903 (2001).

[5] P.W. Shor, "Scheme for reducing decoherence in quantum computer memory," Phys. Rev. A, **52**, R2493-R2496 (1995).

[6] R. Laflamme, "Perfect Quantum Error Correcting Code," Phys. Rev. Letters **77**, 198-201(1996)

[7] C.H. Bennett, D.P. DiVincenzo, J. Smolin and W.K. Wootters, "Mixed state entanglement and quantum error correction," Phys. Rev. A **54**, 3824-3851 (1996).

[8] C.H. Bennett, G. Brassard, S. Popescu, B. Schumacher, J.A. Smolin and W.K. Wootters, "Purification of noisy entanglement and faithful teleportation via noisy channels," Phys. Rev. Letters **76**, 722-725 (1996).

[9] A.R. Calderbank and P.W. Shor, "Good quantum error-correcting codes exist," Phys. Rev. A. **54**, 1098-1105 (1996).

[10] L.K. Grover, "A fast quantum mechanical algorithm for database search," Proceedings of the Twenty-Eighth Annual ACM Symposium on Theory of Computing, 212-219, Philadelphia, PA, (May, 1996).

[11] P.W. Shor, "Quantum computing," Documenta Mathematica, vol. Extra Volume ICM, pp. 467-486, 1998

[12] C.H. Bennett and P.W. Shor, "Quantum information theory," IEEE Transactions on Information Theory, **44**, 2724-2742 (1998).

[13] W.K. Wootters and W.H. Zurek, "A single quantum cannot be cloned," Nature, **299**, 802-803 (1982).

[14] A. Einstein, B. Podolsky, and N. Rosen, "Can Quantum-Mechanical Description of Physical Reality Be Considered Complete?" Phys. Rev. **47**, 777-780 (1935).

[15] B. Schumacher, "Quantum coding," Phys. Rev. A **51**, 2738-2747 (1995).

[16] C.H. Bennett, "Purification of Noisy Entanglement and Faithful Teleportation via Noisy Channels," Phys. Rev. Letters **76**, 722 (1996).

[17] R.W. Hamming, "Error Detecting and Error Correcting Codes," Bell System Technical Journal, 29:147-160, April 1950.

[18] R.C. Singleton, "Maximum distance q-nary codes," IEEE Transactions on Information Theory, 10:116-118, April 1964.

[19] N.J. Cerf, "Information-theoretic interpretation of quantum error-correcting codes," Phys. Rev. A **56**, 1721 (1997).

[20] P.W. Shor and J. Smolin, "Quantum error-correcting codes need not completely reveal the error syndrome," quant-ph/9604006.

[21] A.M.Steane, "Error Correcting Codes in Quantum Theory," Phys. Rev. Letters **77**, 793 (1996).

[22] A.M.Steane, "Multiple Particle Interference and Quantum Error Correction," quant-ph/9601029.